Structures 80 (2025) 110113

Contents lists available at ScienceDirect

Structures

journal homepage: www.elsevier.com/locate/structures

Derivation of fragility curves from non linear dynamic analyses for URM school buildings

S. Giusto, A. Brunelli, S. Lagomarsino, S. Cattari *

University of Genova, Genoa, Italy

ARTICLE INFO

Keywords:
Damage levels
Masonry
Equivalent frame models
EMS98 scale
Interstorey/roof drift thresholds

ABSTRACT

Fragility curves constitute an essential tool in risk studies. Together with the hazard representation and exposed assets databases, they are used to provide an estimate of physical or economic losses. This is typically achieved by introducing consequence functions, which correlate the probability of reaching specific damage levels (DL) – estimated via the fragility curves – with the losses under consideration. Although the physical meaning of DL is well established in engineering practice and various references are available in the literature and shared by the scientific community (like the damage grades and definition introduced by the European Macroseismic Scale), the ways adopted in mechanical-analytical, mechanical-numerical and empirical approaches for converting these principles and thus deriving fragility curves are multiple. That constitutes uncertainty in risk studies which still lacks a consensus on the scientific literature. In this context, the paper explores converting and interpreting the huge amount of data provided by three-dimensional models analysed through nonlinear dynamic analyses (NLDA) into synthetic DLs. One of the main novelties of the procedure is that, differently from the most common approach in numerical methods, it does not require the introduction of inter-storey or roof drift thresholds – conventionally defined *a priori* – to associate the attainment of DLs. The paper focuses on existing unreinforced masonry (URM) buildings. Specifically, seven different URM structures, inspired by real schools, are analysed adopting the equivalent frame modelling approach. The software package adopted – i.e. Tremuri – has been extensively validated in strong nonlinear range in previous research. The analysed buildings were selected based on their comprehensive documentation of geometric and mechanical characteristics, but the methodology applied has general validity. A Cloud-based approach, refined through the combined use of Incremental Dynamic Analyses is adopted to derive the fragility curves, which are compared with other references available in the literature. The proposed approach revealed quite effective and replicable. Moreover, the results gathered through accurate NLDAs are also processed to establish reference values of inter-storey or roof drift thresholds to be used in more simplified approaches (e.g. based on the use of SDOFs system or mechanical-analytical models).

1. Introduction

Fragility curves play a crucial role in seismic risk evaluations, as they represent the vulnerability component and provide a probabilistic estimate of reaching a certain damage level given a specific seismic intensity. Fragility curves commonly adopt a lognormal format and refer to a discrete representation of damage levels. This format is convenient and effective, reducing the problem of reliably estimating the median intensity measure corresponding to the onset of a specific damage level, along with its associated dispersion.

Various methods can be used to develop fragility curves [34,36,104,114,129]. Based on existing literature, the available approaches can be roughly categorized into the following main types:

- Empirical fragility curves derived from post-earthquake surveys.
- Mechanical-Analytical or Mechanical-Numerical fragility curves derived from the seismic response simulations of asset classes or individual archetypes.
- Hybrid fragility curves derived from a combination of the above methods.

Examples of pure empirical fragility curves are those developed by

* Correspondence to: University of Genova - Dept. of Civil, Chemical and Environmental Engineering, Italy.
E-mail addresses: sofia.giusto@edu.unige.it (S. Giusto), andrea.brunelli@edu.unige.it (A. Brunelli), lagomarsino.sergio@unige.it (S. Lagomarsino), serena.cattari@unige.it (S. Cattari).

https://doi.org/10.1016/j.istruc.2025.110113
Received 27 December 2024; Received in revised form 19 August 2025; Accepted 29 August 2025
Available online 8 September 2025

[106] and [52]. Among mechanical-numerical approaches, in the last decades, several mechanical-numerical methodologies have been proposed for the development of fragility curves, spanning from complex analysis of three-dimensional numerical models [5,12,30,64,81,123], to more simplified and expedited methods [35,64,91,105,115,125,128]. An example of a recent automated approach for deriving fragility curves at the urban scale is the META-FORMA-XL procedure, which addresses masonry aggregates through archetype-based numerical analyses while accounting for typological and mechanical uncertainties [107]. Mechanical–analytical approaches typically employ simplified models that require only a limited number of geometric and mechanical parameters, making them particularly efficient due to their low computational effort and their ability to explicitly account for the large variety of features of existing buildings. Examples for unreinforced masonry (URM) buildings, which this paper focuses to, are the First-M PRO and DBV-masonry methods, illustrated and critically compared in Giusto et al. [54], addressed to the in-plane response of URM walls, and that presented in [31], instead focused on the assessment of their out-of-plane response. Finally, examples of hybrid approaches are: the heuristic model developed by [70] that combines the expertise that is implicit in the European Macroseismic Scale (EMS-98, [56]) with the advantage of relying on observed data; the method proposed by [111, 110] that combines observational expert-judgment and mechanical approaches; the VULNUS method [75] based on the integrated use of mechanical-analytical and macroseismic approaches. An interesting example of risk assessment at urban scale in which fragility curves derived from different approaches are used and compared is provided in [29].

All methods have advantages and drawbacks, making it challenging to identify the optimal approach. For example, the empirical approach has the pros that provides valuable insights into building vulnerabilities based on real-world observations but the cons that often entails limitations related to data quality, sample size, and generalizability, which should be carefully considered in seismic risk assessments. The mechanical-analytical and mechanical-numerical approaches offer the benefit of a mechanical understanding of building vulnerability and allow to implement performance-based assessment principles (also more flexible in considering a wider set of intensity measures) but the cons that entail challenges related to the potential limitations in reproducing all possible failure modes and to computational burden. In addition, it is important to note that these methods differ in their ability to explicitly estimate the various sources of uncertainties that contribute to the dispersion (e.g. that associated with the seismic input characterization and record-to-record variability, the structural capacity description, the damage level definition). Recent experiences in the literature have discussed the achievable results comparing different approaches while also highlighting the advantages of integrating multiple methods in national-scale risk assessments [19,44,61,102,36].

Within this context and among the possible alternatives, the paper focuses on the derivation of fragility curves according to a mechanical-numerical approach based on the execution of NonLinear Dynamic analyses (NLDAs) on 3D model with special reference to the URM buildings. Specifically, research questions faced in the paper are developed with reference to the analysis of seven school buildings, selected because they are representative of the Italian school building stock.

Deriving fragility curves through a mechanical-numerical approach involves several issues that need to be tackled, including:

a. Selection of time histories.
b. Selection of the method for performing NLDAs.
c. Definition of efficient and sufficient intensity measure (IM) for synthetic description of seismic input.
d. Availability of appropriate constitutive laws capable of describing the nonlinear hysteretic response of structural elements and different damage mechanisms that may affect the building.
e. Choice of the most robust engineering demand parameters (EDPs) to interpret the structural response and correlate it to the attainment of damage levels.

Some of the above points cut across different structural types (masonry, reinforced concrete and steel) and have been already discussed in the literature. Regarding the time histories, various literature papers discuss the need of an appropriate selection of the ground motion time-history records as well as defining appropriate nonlinear hysteretic models [37,39,47,65,95]. Moreover, various tools already available in the literature have improved the process of selecting seismic inputs [58, 59,78,112,119]. Regarding the IM, selecting the most suitable measures for probabilistic seismic demand analyses is of paramount importance, as emphasized in prior studies [45,77,84,85,113]. Regarding the method to perform NLDAs, various methodologies to derive fragility curves are accessible in the literature, including the Incremental Dynamic Analysis (IDA) method [100,124], the Multiple Stripes Analysis (MSA) method [62], and the Cloud Method [6,63]. Interested readers may refer to these works for a more in-depth discussion of the topic. In particular, this paper faces the issue b), by employing as an approach to perform NLDAs the CLOUD+IDA method and by adopting as accelerograms' selection the one finalized in [78] which was extensively applied in the MARS project [20,19,82].

Concerning issue d), advancements in nonlinear constitutive laws also able to describe the hysteretic response of masonry panels have enhanced the accuracy of simulating complex URM building responses [10,24,76,98,126]. In the paper, the modeling in the nonlinear field of the examined structures is performed by adopting the equivalent frame (EF) approach and in particular the Tremuri software [76]. The choice of the EF approach is justified by its computational efficiency, which is an important requirement for the investigated NLDA-based approach as already demonstrated in a variety of literature experiences [13,24,38, 97]. The use of the Tremuri software is corroborated by several validations performed on multiple structures whose comparison with the actual response (also enhanced through seismic monitoring data) was also available [2,13,20]. A particularly relevant validation is documented in [13] which describes the case study of the Visso' school monitored by the Italian Department of Civil Protection. This structure is of special interest because it suffered severe damage, enabling validation of the modelling strategy and constitutive laws well into the highly nonlinear range. This is a crucial aspect, as the derived fragility curves also cover very high damage level up to the near collapse state. The EF approach adopted enables the global response associated with the activation of in-plane damage modes of walls, thus assuming that the activation of possible local mechanisms is inhibited. This assumption is justified, for the case studies examined, since a box-like behavior with rigid floors and the presence of reinforced concrete beams at floor level characterize them. Actually, these features are rather recurrent in the case of school buildings [26,19]. The issue inherent the integration of the global in-plane response with the out-of-plane response, which is relevant for URM existing structures but out of the scope of this paper, is addressed in other works [1,101,116].

The issue e) constitutes one of the main novelties of the paper. Specifically, the paper explores the conversion and interpretation of the huge amount of data provided by three-dimensional models analyzed through NLDA into synthetic DL. To this aim, differently from the most common approach in numerical methods, it doesn't require the introduction of inter-storey or roof drift thresholds conventionally defined *a priori* to associate the attainment of the DL and, instead, it directly refers to concepts related to the severity and spread of damage occurred. The approach is conceptually consistent with the engineering process adopted to assign DLs in actual seismic damage surveys and starts from the original proposal introduced in [20].

Following the aforementioned research questions, Section 2 illustrates the iterative procedure developed for refining the execution of CLOUD+IDA method together with the approach proposed for assigning

the DL from NLDA' output data. The analyzed buildings together with the corresponding numerical models are extensively described in Section 3. They have been selected due to their comprehensive documentation regarding geometric and, in some cases, mechanical features.

Finally, the main outcomes achieved are illustrated in Section 4. Here the fragility curves that have been derived are presented as well as the impact of possible alternative choices on the DL definition and of the use of iterative procedure used for executing the NLDAs is discussed. Moreover, fragility curves derived according to the proposed approach for assigning the damage level are also compared with the results achievable from a more traditional approach based on the use of roof drift thresholds. Section 5 presents a comparison between the derived fragility curves and those available in selected references. Finally, in Section 6 the results are also processed to establish reference values of inter-storey (and roof) drift thresholds. In fact, even if the proposed procedure allows to overcome the use of such EDP, these values may be useful in other applications where analysts are forced to use simplified mechanical-analytical methods which don't allow to have a direct and detailed estimate of the damage at panel scale.

2. Procedure adopted for the derivation of fragility curves

Fragility curves are derived according to a lognormal format, thus requiring for each Damage Levels the definition of the average value (IM_{mi}) and the standard deviation (σ_{mi}) of the selected Intensity Measure (IM) of the input motions causing the achievements of each damage level, as further explained in the following paragraph. In particular, the Peak Ground Acceleration (PGA) has been selected as IM. The probability of exceeding the different damage levels, p_{DLi}, under a certain PGA can be consequently calculated as the probability that such PGA "exceeds" the calibrated lognormal distribution:

$$p_{DLi}=p(DL>DLi|PGA)= \Phi((\log PGA|PGA_{mi})/\sigma) \quad (1)$$

where Φ is the standard cumulative probability function. The value of the standard deviation accounts for the various sources of uncertainty involved in the process and accounted for the method adopted to derive the fragility curve, as further detailed in next sections.

As introduced in Section 1, one of relevant points for deriving fragility curves consists of the selection of appropriate EDPs and the criteria for determining when a specific DL has been reached. This is crucial for ensuring consistency across curves derived from different approaches. The EDP represents a variable or set of variables that can be monitored during the analysis to check the progression of nonlinear response and the attainment of specific performance conditions.

In the field of mechanical-numerical methods, particularly concerning NLDAs to which this paper is focused, the most commonly adopted EDP in the literature is the inter-storey drift or, in some cases, the roof drift. Several studies – primarily for reinforced concrete buildings [64,80,122,130], but also for masonry structures [16,18] - use this option. Such an approach requires defining reference thresholds to establish the transition from one level of damage to the next one. These thresholds usually rely on conventional values proposed in the literature, [17,48] or are defined ad-hoc for the building under examination through the execution of monotonic nonlinear static analyses (NLSA) (see e.g. [86,89]).

Although the peak drift ratio has been demonstrated as a quite good predictor of seismic damage also in recent applications that rely on recorded measurements of monitored structures [88], in the case of URM buildings various proposals in the literature have shown the advantage of considering more than one EDP. For example, in [24,96] the attainment of usability prevention damage (roughly assimilable to DL2) corresponds to the occurrence of the first of three conditions: attainment of a base shear equal to 95 % of the maximum base shear in the pushover curve; attainment of light/ moderate damage in at least 50 % of the piers; and, attainment of collapse (e.g. $DL3_E$ in at least one pier). The first condition necessary requires the execution of a NLSA, the second and third may also directly refer to the damage simulated by NLDAs. [89] explored the use of different EDPs, that is: the maximum inter-storey drift; a weighted average drift calculated as the average of the drifts of all the elements of the critical storey, weighted on their area; the displacements (which can be easily converted in roof-drift values) associated to the attainment of maximum base shear and its degradation to 80 % of its maximum value. According to this work, the thresholds associated to the attainment of this condition are defined on basis of monotonic or cyclic nonlinear static analyses. [73,74,79] developed a multiscale methodology that integrates multiple criteria across different scales, examining damage in masonry elements (piers and spandrels, DL_E), individual wall responses (DL_W), and overall building behaviour through pushover analysis. In [79], the possible drawbacks in adopting conventional threshold values of inter-storey drift are discussed. Specifically, these authors highlighted that defining universal thresholds for all URM walls in existing buildings is challenging due to i) variations in masonry types; ii) the presence of irregular distributions of openings; iii) different damage failure modes (i.e. flexural, shear or hybrid) which can be activated in masonry panels under seismic loads. Concerning the latter, the prevailing damage mode in URM panels depends on several factors including: geometry; slenderness ratio; restraint conditions which in piers are strongly correlated to the response of spandrels; vertical compression level; and mechanical properties of masonry. Different drift thresholds usually correspond to the activation of these different failure modes at the scale of piers. Consequently, due to the potential variation in piers' drift, even located at the same level, inter-storey drift is also affected and variable from one building to another and, also, in the same building, from one level to another. To overcome these limitations, in [79] a new criterion - called "DLmin" check – was proposed. According to this criterion, a DL is reached when all the piers in a storey of a wall reach a DL_E equal to or higher than the one monitored. Regarding the inter-storey drift check, the purpose of this criterion is to identify the potential triggering of a soft storey mechanism. This approach has the advantage of not requiring the definition of inter-storey drift thresholds, but it is based only on the pier behaviour (and their drift), for which more data is available in the literature, consequently allowing for a more robust calibration. Recently, [71] extended the multicriteria approach proposed by [73,74], and [79] to include the activation of damage in diaphragms. Although these proposals allow to extend the concept of using a single EDP and provide improvements on the use of inter-storey drift, they still partially rely on results of pushover curves. Instead, the proposal by [23] allows to completely remove the dependence on NLSA, focusing solely on damage spread concepts which are consistent with those introduced in the EMS98 [56] and applicable in a very effective way in NLDAs. Recently, in [49] similar concepts have been tested also for reinforced concrete structures.

The approach proposed in this paper aligns with [23], further refining some aspects and carrying out a parametrical analysis addressed to explore the sensitivity of results to alternative options in the thresholds assumed for the cumulative rate of damage in walls and damage assignment criteria at pier scale. While a more detailed explanation of these issues is provided in Section 2.1, Fig. 1 aims to provide a general overview of the proposed procedure highlighting its main innovations and key points. The figure refers to the interpretation of results obtained from NLDAs carried out according to the Cloud approach, which is the one adopted in the paper (even if then refined by the combined use of IDA).

The first box of Fig. 1 illustrates a traditional approach, in which roof drift thresholds (easily computed from the top displacement estimated on the numerical models) corresponding to the attainment of given DL attainment, are associated with conventional total base shear values (either in the ascending part of the pushover curve or in the softening part). These thresholds are usually defined executing monotonic NLSAs. The DLs roof drift values are representative of the thresholds that

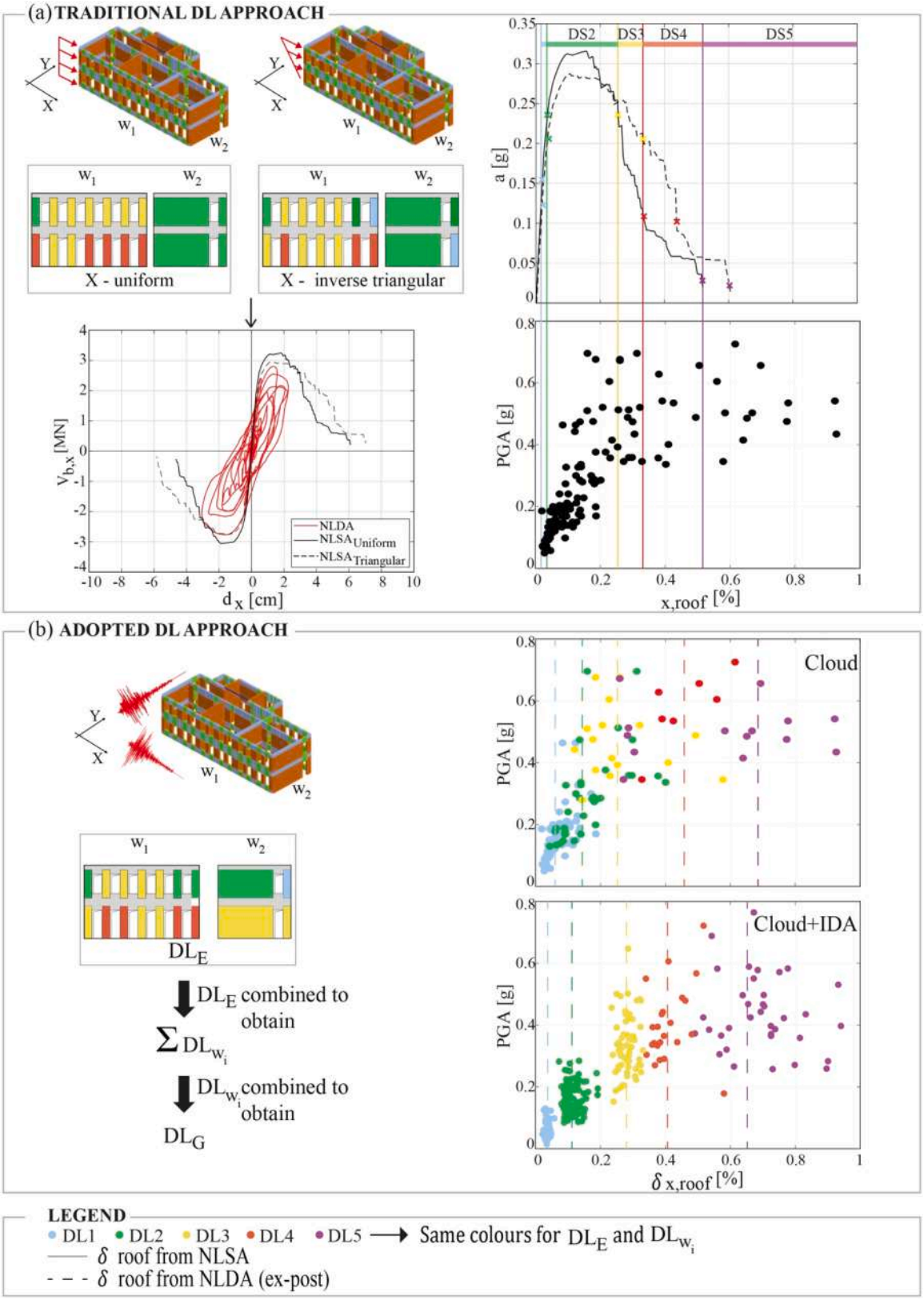

Fig. 1. Sketch of the proposed approach: comparison between the traditional (a) and adopted (b) approach.

separate various Damage States (DSs), which refer to the discrete qualitative description of the overall damage of structural and/or non-structural elements of the building. As known in the literature, the results of a NLSA are sensitive to various factors, like as the applied horizontal load pattern or the control node choice [4,76,90,108]. Thus, this approach presupposes also defining which load pattern is considered the most reliable (as also debated in [89]) or at least adopting conservative criteria (i.e. relying on the lowest roof drift provided by

two load patterns) and performing a sensitivity analysis on the control node (this is especially relevant in the case of flexible diaphragms). Also, the resulting simulated damage depends on these factors, thus the adoption of a set of EDPs which rely on criteria based on the spread of damage cannot overcome such intrinsic simplification of NLSA. In addition, since usually NLSAs consider the application of horizontal forces in one main direction at each time, the simulated damage surely constitutes an approximation of the actual one produced by a real seismic event. Vertical continuous lines in Fig. 1 are associated with the thresholds assumed to be representative of the transition from one DL to the next one.

The second box of Fig. 1-A instead illustrates the use of such thresholds to associate a DL to the results of NLDAs (expressed by dots associated to the PGA of the given i-th record and the maximum roof drift estimated by the numerical analysis). The results of NLDAs are represented by *black* dots in this figure since the association of the DL is made ex-post by comparing the maximum roof drift obtained from the NLDA with the thresholds defined by the NLSA.

Fig. 1-B instead summarises the proposed approach aimed to overcome the limitations of the traditional method by performing bidirectional NLDAs. The dots are *coloured* since the DL is associated directly through the interpretation of damage simulated during the analysis (according to the criteria explained in detail in Section **2.1**). Actually, the values of the roof drift thresholds which correspond to the vertical dashed lines in **Fig. 1** are computed based on results associated with the set of time histories grouped in the same DL. Thus, in this case, the roof drift thresholds are defined ex-post with the aim of establishing reference values when mechanical-analytical models or NLDA on SDOFs are performed, which are not able to provide an accurate picture of the damage at the element scale. While the first graft of **Fig. 1**-B refers to the execution of a traditional Cloud analysis, the bottom graph in **Fig. 1**-B shows the impact of adopting a refined Cloud+IDA analysis as shown in Section **2.2**. As depicted, moving from the two graphs, the values of the roof drift thresholds are further updated. Actually, the refined Cloud+IDA analysis aims to rescale the time history to identify the value of PGA closest associated with the first attainment of the DL which is assumed conceptually consistent with the physical meaning of the deterministic values identified in the pushover curve (continuous line of **Fig. 1**-A).

The two next sections better specify the criteria adopted to assign the DL to each record (Section 2.1) and to implement the Cloud+IDA analysis (Section 2.2).

2.1. Damage level definition

As introduced in Section 2, the procedure adopted in this paper relies on the proposal of [23].

The procedure proposed in [23] was conceived to interpret the damage of buildings that mainly exhibited a box-behavior (i.e. dominated by IP response) and, therefore, with local failure mechanisms extended to a limited portion of the building or none at all. This context is compatible with the main features also of the case studies examined in the paper.

Specifically, the procedure allows the definition of DLs − graduated into five levels i = 1,…5 as proposed in the EMS98 scale − starting from different level scales (i.e. at the panel's scale and macroelement scale, where the macroelement is intended as an assemblage of components like as vertical walls or diaphragms) with the ultimate goal of assigning the global damage to the investigated building (DLi_G). The damage at smaller scales (i.e. at panel or macroelement scales) is also set on five levels (i.e. DLi_E for panels and DLi_W for walls) although the physical meaning varies from one scale to another. The only one that strictly conceptually refers to the description of EMS98 is the global damage, DLi_G. The damage at lower scales is progressively combined and interpreted to arrive at the DLi_G; the starting point is the damage simulated at the panel scale (i.e. piers and spandrels).

In [23] specific proposals were introduced to interpret the linguistic descriptions of EMS98 [56] using analytical and reproducible criteria. Specifically, the concept of "spread of damage" was included by specifying the percentage of walls required to reach a given $DLi_{W,}$ which affects the performance of the structure corresponding to a certain DLi_G.

This paper further investigates the proposal of [23] by:

- refining the criteria adopted to compute the DLi_W
- performing a parametric analysis on various options for attributing the DLi_E, for combining results and defining DL_G.

Concerning the first issue, this paper calculates the damage in the wall (DLi_w), defined:

- as the mean value of average damage of each level (L) of a given wall ($DL_{Lw,mean}$) if the $DLL_{w,mean}$ of each level is less than or equal to 2.
- otherwise, DLi_w is the maximum value of $DL_{Lw,mean}$ of that wall.

This differentiation allows for the consideration of peak damage concept at higher damage levels.

The $DL_{Lw,mean}$ is determined as the average of DLi_E of the piers at that wall level, weighted by the resistant area of the piers. The DLi_E is assigned based on the drift achieved at the element scale (Fig. 2a). Although robust reference drift values are available in the literature due extensive experimental results (e.g. [3,7,9,55,87,99,103,127]), some uncertainty is intrinsic in the process. This is why different possible alternatives have been considered moving a bit the position of DLi_E associated to $DL2_E$ and $DL3_E$. In particular, the alternative options for $DL2_E$ correlates it to the yielding point (δ_y) of the shear-drift relationship that describes the nonlinear response of panels.

That is graphically represented in Fig. 2b and summarized in Table 1 (first two columns).

Fig. 3 compares the attribution of DLi_w using in one case the maximum of $DL_{Lw,mean}$ in that wall (defined $DL_{w,mean}$) and in one case the average of $DL_{Lw,mean}$ (defined $DL_{w,max}$). The figure illustrates a simplified scenario where all piers have the same resistant area. To convert DLi_w from a continuous value to a discrete number, the binomial distribution method outlined in [75] is used: 1 if $0.7 < DL_w \leq 1.6$; 2 if $1.6 < DL_w \leq 2.5$; 3 if $2.5 < DL_w \leq 3.4$; 4 if $3.4 < DL_w \leq 4.3$; 5 if $4.3 < DL_w \leq 5$; otherwise, 0.

This comparison served to assess that the $DL_{w,max}$ was more representative of a peak value and thus usable to obtain the DLi_w associated with higher damage even at one level ($DL_{Lw,mean}$). While the $DL_{w,mean}$ represents widespread, but not high damage.

Fig. 3 shows the differences produced between the two alternative estimates, particularly when there is a notable disparity in damage levels achieved. Considering the $DL_{w,max}$ for higher $DL_{Lw,mean}$ helps prevent underestimating damage if a soft storey mechanism has been triggered. Greater differences are expected in taller buildings compared to shorter ones.

The defined procedure involves constructing the cumulative DLi_w calculated according to the procedure explained in the previous paragraphs. The cumulative of DLi_w ($\sum DLw$) is weighted on the resistant area of all the piers in that wall, and they are calculated for the five damage levels. The thresholds for defining the attainment of the building-scale damage level (DL_G=DL of the building) are shown in Table 2. Each line introduces the criteria adopted to establish the attainment or exceeding a given DL; the integration of criteria of a given line with the next one allows to strictly define the attainment condition of a given DL. For example, the attainment of $DL4_G$ is associated to this condition $\sum DL4_w \geq 0.30$ provided that $\sum DL5_w$ is lower than 0.5.

For $DL1_w$ and $DL2_w$, the cumulative of DL_w is done by considering all the walls of the building without differentiating them by direction. Instead, starting from $DL3_w$ the directionality of the walls is considered, so two separate cumulative of DL_w are computed for the two directions. In this case the maximum reached damage is assumed as reference to assess the global building-scale damage.

There can be many calibration options for the definition of the DLs to

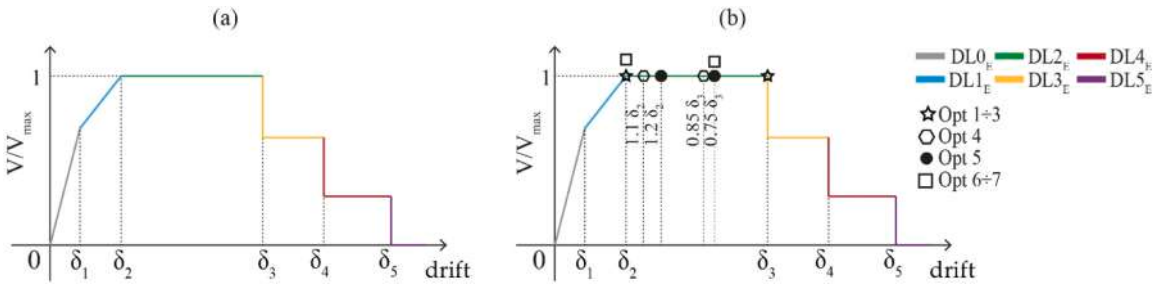

Fig. 2. – Constitutive law of masonry piers in shear failure (a), and modifications of drift thresholds according to explored options (b).

Table 1
Description of the seven analyzed options (Opt) for defining the DL from NLDAs.

Opt	Drift threshold $DL2_E$	Drift threshold $DL3_E$	$DL1_w$ threshold	Verification Criteria for DL2	$DL4_w$ to define DL5
1	δ_y	δ_3	30 %	directional	Yes
2	δ_y	δ_3	30 %	global	Yes
3	δ_y	δ_3	40 %	global	Yes
4	1.1 δ_y	0.85 δ_3	30 %	global	Yes
5	1.2 δ_y	0.75 δ_3	30 %	global	Yes
6	δ_y	0.75 δ_3	30 %	global	Yes
7	δ_y	0.75 δ_3	30 %	global	NO

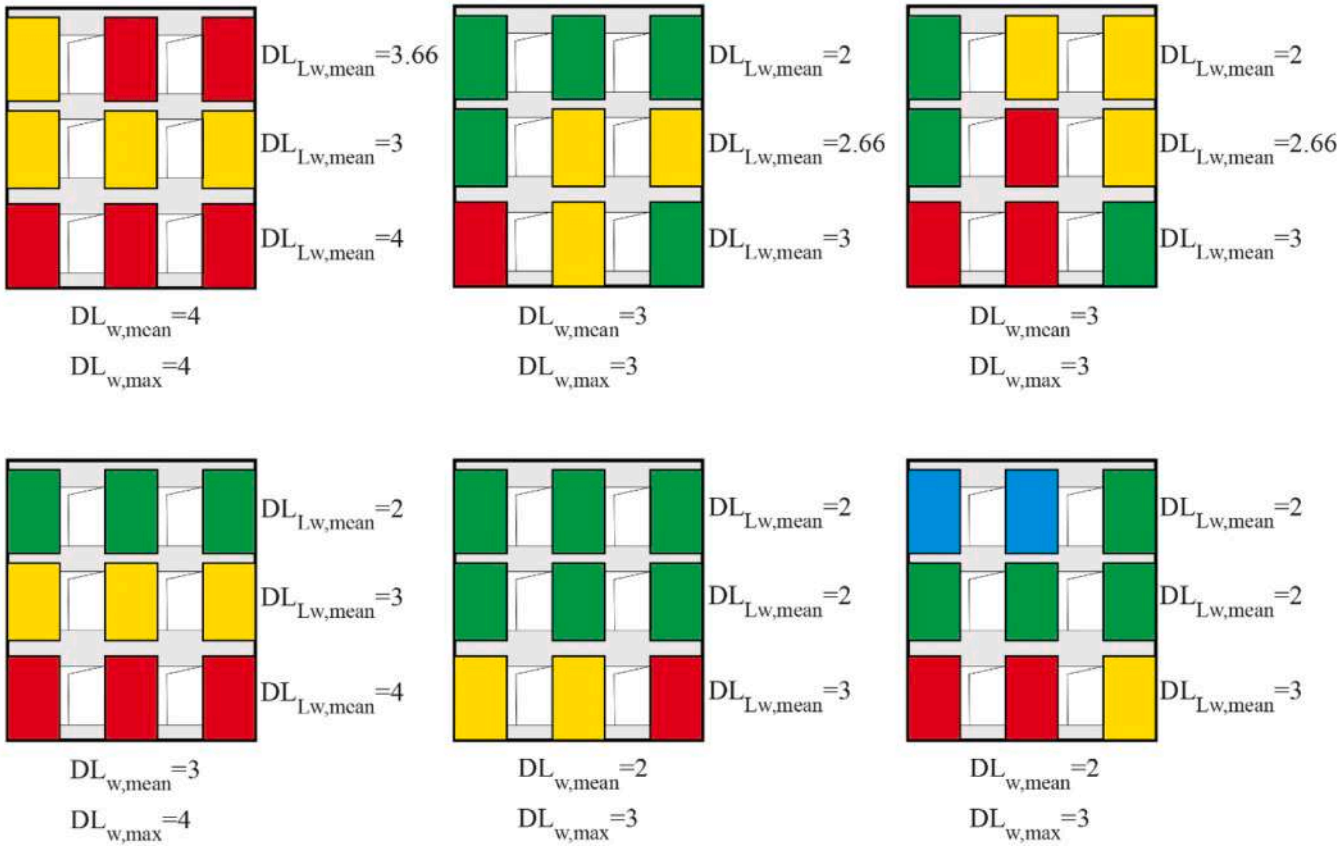

Fig. 3. Simplified scheme of wall damage calculation for different damage configurations.

be adopted, in particular, seven options were investigated as shown in Table 1.

This verification can be done either by considering all walls collectively (a global verification, as with DL1) or directionally, as done for higher DLs. As shown in Fig. 2b, an approach was chosen to anticipate the activation of $DL3_E$, while also considering a delay of 10 % or 20 % in the $DL2_E$ threshold. Finally, for controlling the activation of DL5, it was chosen to test whether the diffusion of $DL4_w > 70$ %. Opt. 7 corresponds to the final procedure later adopted in the paper.

The result of this sensitivity analysis for two case studies is reported in Section 4.1.

Table 2
Exceedance thresholds for defining building-scale damage.

DL_G	
$DL_G \geq 1$	$\sum DL1_w \geq 0.30 \vee \sum DL2_w \geq 0.15$
$DL_G \geq 2$	$\sum DL2_w \geq 0.35 \vee \sum DL3_w > 0$
$DL_G \geq 3$	$\sum DL3_w \geq 0.50 \vee \sum DL4_w > 0$
$DL_G \geq 4$	$\sum DL4_w \geq 0.30 \vee \sum DL5_w > 0$
$DL5_G$	$\sum DL5_w \geq 0.50$

The various options aim to parametrically analyse some threshold values, particularly those associated with the definition of $\sum DL1_w$ and the verification of DL2.

2.2. Implementation of the refined cloud and IDA procedure

The NLDAs were performed using the selection of records made by [78] that selected accelerograms in the SIMBAD database, [121,120] according to the maximum moment magnitude and rigid soil. The epicentral distance range of SIMBAD contains almost exclusively records up to about 30 km distance so no specific filtering was made in terms of distance. 85 accelerograms are real, while 40 are rescaled in frequency to be representative of longer return periods (5000 and 10000 years). The same dataset of signals has been already tested for developing other fragility curves within the context of MARS project [19].

The maximum PGA value between the two components of accelerograms is the defined IM of each analysis.

This approach allows the construction of five fragility curves that represent a specific DS, though they do not capture the precise threshold at which that damage level is reached. This means that an analysis might have just exceeded the threshold or be close to the next damage level, yet both cases are currently treated the same in the statistics.

To accurately capture the PGA value that leads to reaching the threshold for each damage level, an iterative procedure was developed and implemented in a MATLAB script. Starting from the initial PGA value at iteration zero (the value without iteration, as in the cloud analysis discussed in previous sections), this procedure rescales the event for each i-th analysis by applying an amplifying factor (f_2) to capture the upper threshold and a reducing factor (f_1) to capture the threshold of the DL relevant to the i-th analysis.

The procedure consists of two steps:

STEP 1

The first iteration rescales the PGA by two factors, namely f_1 and f_2, whose value limits are based on expert judgment following the extensive application to the selected case studies, while others are driven by the intention to restrict the amplifying/reducing factors and to avoid unrealistic physical alterations of the signals. Recently, [14,15] faced the issues related to selection and scaling of ground motions, also verifying the rules proposed in the Eurocode 8. In particular, the following practice-oriented formulas for the f_1 and f_2 factors are proposed to facilitate the application of the procedure:

$$f_1 = \max\left[0.67; \min\left(\frac{1}{1+(\alpha_{DSi}-1)(\varphi_{DSi}-1)}; \frac{1}{1.1}\right)\right] \quad (2)$$

$$f_2 = \min\left[1.74; \max\left(\alpha_{DSi} + \frac{\varphi_{DSi}}{1-\alpha_{DSi}}; 1.1\right)\right] \quad (3)$$

Where:

- α_{DSi} represents the ratio of the IM_{50} between the DS of interest and the next DS. For the sole purpose of making an initial rescaling it is proposed to assume: $\alpha_{DS1} = \alpha_{DS2} = 2.8$, $\alpha_{DS3} = 1.8$, $\alpha_{DS4} = \alpha_{DS5} = 1.3$.These values were established on basis of the application made on several buildings.
- φ_{DLi} is the ratio between the cumulative DSi value and the threshold defined in Table 2. This allows for a scaling factor that reflects the extent to which the analysis surpasses the reference threshold at a given damage level.

The different reference thresholds used in defining the f_1 and f_2 factors are intended to prevent scaling from being either too small, which would make the analysis essentially identical to the previous one, or too large, which would make it incompatible with the initial analysis due to scaling being applied in terms of PGA rather than frequency. These reference values have been proposed after a calibration based on the parametric analysis carried out of the selected case studies and was addressed to guarantee a limited maximum number of iterations (accepting a maximum error of 5 % is maximum 9 iterations) for reducing the computational burden.

STEP 2

From the second iteration, the procedure splits into two different possibilities:

- if the analyses change DS (either to a higher DS when scaling forward or a lower DS when scaling backward) an iterative bisection process is done. The convergence is achieved when the difference between the PGA of the current and threshold-crossing analyses is less than 5 %, relative to the PGA of the initial analysis.
- if the DL threshold has not yet been exceeded, the scaling continues by defining a new scaling factor, calculated as twice the PGA of the current analysis minus the PGA of the previous one. This process is repeated until one of the following conditions occurs:

-the DS changes and so the bisection process is carried out as explained in the previous step.

-the scaling factor reaches an extreme value: below 1/3 when scaling towards a lower DS, or above 2.5 when scaling forward. These values are also compatible with those recommended by Eurocode 8.

In the latter case, the analysis is deemed unrepresentative of the DL threshold and is therefore disregarded.

This iterative procedure requires processing the results of the NLDAs using implemented MATLAB code, setting up a new series of analyses until convergence of that analysis. Analyses falling within DS0 are scaled forward only to establish the DL1 fragility curves, and those within DS5 are scaled backward solely to define the DL5 fragility curves. All other analyses are scaled both forwards and backwards, yielding not only IMs that are indicative of surpassing a DL, rather than merely reaching a specific Damage State, but also a larger dataset of analyses within each DL.

3. URM school buildings stock and modeling assumptions

In this paper, seven URM school buildings were analyzed. Each building was chosen as representative of the Italian masonry school building stock [19]. According to the inventory of the Italian Ministry of Education, Italian URM schools are characterized by a number of stories rarely higher than three and the presence of rigid floors; moreover, in the case of ancient ones, a significant inter-storey height and great distance between transverse walls are recurring features [21].

Four school buildings have been selected from the Friuli-Venezia Giulia (FVG) regional database provided by the University of Trieste (primary school in Mortegliano (UD), secondary school in Pradamano (UD), primary school in Ovaro (UD) and secondary school in Cividale de Friuli (UD)) [54].

Then, additional three case studies were selected from the regional database provided by the University of Naples and Genoa (see [94]). This database groups data collected during the support activity made by the ReLUIS consortium and Italian Department of Civil Protection [41,42], requested by the Reconstruction Commissioner, nominated after the 2016/2017 Central Italy earthquake. More specifically, the three

schools are inspired by some schools located in Visso (MC), Caldarola (MC) and Montegallo (AP).

In this paper, each school building was analyzed only considering the configuration in which reinforced concrete beams and rigid diaphragms are present in the building, that is quite recurring in school buildings.

Based on the taxonomy defined in the MARS-School project [19] a first classification was done. More specifically, the MARS-taxonomy for schools considers: masonry typology (e.g., regular, irregular); age of construction (before 1920, 1921–45, 1946–60, 1961–75, after 1976); number of stories (i.e., 1,2,3, >4); plan area (i.e., <500 m^2, 500–1000 m^2, 1000–2000 m^2, 2000–5000 m^2, and >5000 m^2); diaphragm type (e.g., concrete slab with clay units, wooden floor). This classification was useful for making some comparisons with other fragility curves available from literature (see Section 5).

3.1. Geometrical and structural features and mechanical parameters

The first case study of the FVG region is the Mortegliano School, built in the period 1921–45. The structure has a regular planimetric shape, which can be categorized as quadrangular with projections. The building is also regular in elevation, with 2 storeys above ground, and consists of a prevalent masonry type of uncut stone with uneven thickness faces and the presence of three masonry walls of solid brick and lime mortar. In addition, the uncut stone masonry is characterized by the presence of lathings, while solid brick masonry is characterized by a good transverse connection between orthogonal walls.

The second case study of the FVG region is the Pradamano School, built in the period between 1946 and 1960. The structure has a Planimetric shape classified as elongated rectangular, while the elevation development is regular, characterized by 2 floors above ground. The masonry type that makes up the structure is unique and is classified as solid brick and lime mortar masonry with good mortar characteristics.

The third case study of the FVG region is the Ovaro School, also built in the period 1946–60. The structure has an irregular planimetric shape and is also irregular in elevation being characterized by 2 floors above ground and 1 semi-basement floor in one portion. The prevailing masonry type is of cut stones consolidated through mortar injections.

The fourth case study of the FVG region is the Cividale del Friuli School, a building built before 1920. The structure has an irregular planimetric shape and is also irregular in elevation, with 4 total floors, of which one body extends only to the third floor. The masonry type is uniform along the structure and consists of cut stones with good mortar characteristics. The case is certainly a significant prototype building, useful to describe medium-rise school buildings and characterized by a significant size. Moreover, this structure is dynamically and permanently monitored by the Seismic Observatory of Structures (OSS) managed by the Italian Department of Civil Protection [43]. The data available to the OSS on the identification of the dynamic properties of the structure were used for initial calibration of the model, having, moreover, verified that employing the reference values of the Italian Circular (see [32]) of the Italian Technical Standards for Construction (see [92]) the error on the estimation of frequencies was very limited.

Table 3 gives an overview of the analyzed set in terms of construction age, number of floors, plan shape, area, plan configuration, inter-storey height and wall thickness.

The fifth case study is the Visso School (construction period 1921–45, 2 storey, area 500÷1000 m^2), inspired by the real school in Visso (MC, Italy), a structure that was monitored by OSS until 2017 and subsequently demolished after the severe damage suffered after the Central Italy earthquake in 2016/2017. A detailed list of the structural details of Visso' school is available from other research projects [13,25,23,28]. This structure is characterized by a T-planimetric shape, with two floors above ground. The building is regular in elevation and consists of a prevailing masonry type of cut stone with good texture, with the presence of some masonry pillars of solid brick and lime mortar. In Table 3 the main structural characteristics of the building are reported.

The sixth case study was inspired by the Caldarola School (construction period 1921–45, 2 storey, area 500÷1000 m^2). This building has been demolished due to the severe damage suffered during the seismic sequence in central Italy in 2016/2017. The uncut stone masonry typology that characterizes that building in its actual configuration was of particularly poor properties [22]. The main body of the building is elongated rectangular and has two levels in elevation.

The seventh case study was inspired by the Montegallo School (construction period 1946–60, 3 storeys, area 25÷500 m^2). The third school building was built around the 1960s, which is more recent than the two previously analyzed buildings that dated back to the 1930s. The structure has a regular planimetric shape but has irregularities in elevation as it is two stories above ground, but with a portion of the building having an additional semi-basement floor. The masonry is of cut stone with brick recourses. In Table 3 the main structural characteristics of the building are reported.

In Fig. 4, each school's plan is depicted along with accompanying photos to offer a comprehensive overview of the building.

3.2. Numerical models

The 3D structural models of examined school buildings were generated through the equivalent frame (EF) approach and by adopting the Tremuri software [76]. The EF modeling, among other possible choices suited for masonry structures [33], is proposed not only in literature [76] but also explicitly recommended by some Codes [46,92]. This approach reduces the number of degrees of freedom and therefore allows performing NLDAs of three-dimensional masonry structures with a reasonable computational burden [24]. The Tremuri software [76] was largely validated in previous studies, including numerical simulations of the seismic response of well-documented experimental tests on laboratory specimens and real buildings affected by earthquakes (for which monitoring system records were also available) [13,38,97]. Moreover, apart from the numerical studies aforementioned, the efficiency of this modelling strategy has been proved in various works aimed at developing fragility curves [1,21]. It is worth noticing the

Table 3
General data of analysed school buildings.

ID school	Case Study	Age	N floors	Area [m^2]	Plan configuration	Inter-storey height [m] min-max	Wall thickness [m] min-max
CS1	Mortegliano	1921–45	2	< 500	Quadrangular with projections	4.70–4.90	0.25–0.40
CS2	Pradamano	1946–60	2	< 500	Elongated rectangular	3.80	0.25–0.50
CS3	Ovaro	1946–60	3	500–1000	Irregular	2.90	0.20–0.95
CS4	Cividale del Friuli	Before 1920	4	500–1000	Quadrangular with projections	3.81–4.32	0.24–1.50
CS5	Visso	1921–45	2	500–1000	T-shape	4.30–4.40	0.30–0.71
CS6	Caldarola	1921–45	2	500–1000	Elongated rectangular	4.43–4.44	0.20–0.75
CS7	Montegallo	1946–60	3	< 500	Quadrangular with projections	2.42–3.16	0.16–0.55

Fig. 4. Plan shape and photos of the analysed schools.

equivalent frame schematization is particularly suitable if the wall geometry and the distribution of the openings in the building are characterized by a certain regularity, in particular about the alignment of the openings. The 3D view of EF models of the analyzed schools is reported in Fig. 5, where the piers are depicted in orange, while the spandrels are shown in green. These panels are interconnected by rigid nodes (shown in cyan in Fig. 5).

The numerical masonry building models were developed in previous

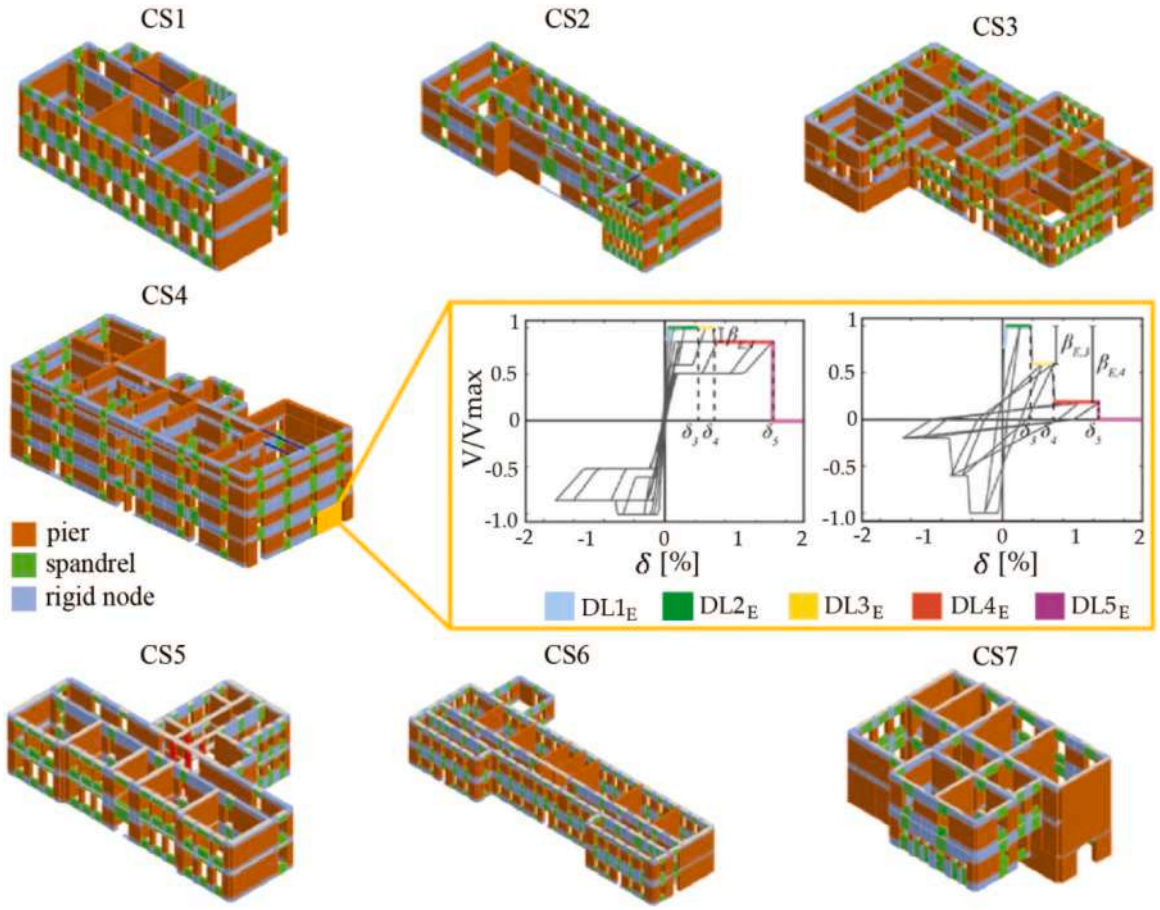

Fig. 5. – Equivalent frame models of the several cases examined and examples of backbone and hysteretic response for masonry piers under flexure (left) or shear (right).

research works, in particular CS5 model in [13] and the CS6 model in [20]. In these two works also a validation of the equivalent frame model reliability was made.

For performing NLDA, the multilinear constitutive law developed by [27], has been adopted to simulate the in-plane nonlinear response and the hysteretic behaviour of masonry panels.

The shear-drift relationship in Tremuri software [76], based on a piecewise-linear constitutive law for panels, embodies a phenomenological approach. It enables straightforward monitoring of the damage levels (DL_E) attained in each deformable structural element (piers and spandrels) subjected to cyclic loading, facilitating assessment of stiffness and strength deterioration. Additionally, the phenomenological approach effectively replicates a hysteretic response, allowing for differentiation among various failure modes (predominantly flexural, shear, or mixed) and different behaviours of piers and spandrels.

Specifically, the attainment of a damage level in the structural element is tracked by surpassing drift thresholds set by the analyst, which vary for spandrels and piers and are adjusted based on the failure

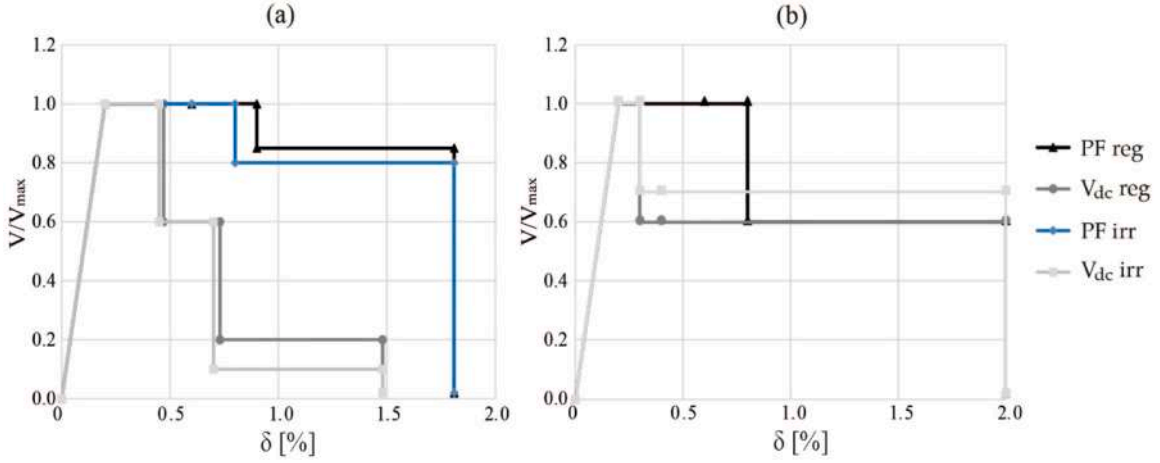

Fig. 6. Constitutive laws for (a) piers and (b) spandrels, assumed according to [96] and [69] for damage levels up to $DL4_E$, and the ones of [13] for damage level $DL5_E$.

mode (whether flexural, shear, or hybrid). These thresholds in the numerical model effectively mirror the real-world progression of damage, such as crack widening and propagation.

In this paper, the constitutive laws assumed to describe the resistance to shear (V_{dc}) or flexural (PF) failure mechanisms of the masonry types are reported in Fig. 6, and are coherent with literature values [13,71, 96], in which the drift (δ) and strength decay values were calibrated to be as representative as possible of reality and were consistent with the up-to-date experimental evidence as reported in some databases [87, 103,127]. The behaviour of the spandrels as shown in Fig. 6b does not vary in the case of PF damage between irregular and regular masonry.

The values assumed as mechanical parameters (e.g. shear strength (τ_0), masonry compressive strength (f_m), Young modulus (E) and specific weight (w)) for the masonry type schools are reported in Table 4 and calculated based on the reference range of variation proposed in Table C8.5.II of [32].

Additionally, corrective coefficients (Table C8.5.II in [32]) were considered, where reasonable for the specific features of the examined school buildings. These coefficients account for specific features influencing masonry response, such as good quality mortar, effective transversal connections between walls, and the presence of courses enhancing horizontal layer alignment [8,67]. Using this approach, plausible ranges of mechanical parameters were adopted for each school, in which the minimum value aligns with the minimum proposed in [32] and the maximum value corresponds to the Code's maximum proposal, to which all the possible corrective coefficients were applied. At the end, for executing the NLDAs, the median values (as reported in Table 4) of the mechanical parameters within the parameter range were adopted.

As aforementioned, for CS5 and CS6 a very accurate validation even in a strong nonlinear range was made in some precious works [13,20]. Instead in this paper, the data of ambient vibration tests available from OSS were used to verify the reliability of c the model of CS4 school at least in linear range.

The ambient vibration measurements refer to approximately 40 min of data acquisition collected in July 2016. Identification through Frequency Domain Decomposition allowed for clear identification of the structure's first five modes. Specifically, the first three modes of the structure at 4.4 Hz, 4.55 Hz, and 4.8 Hz can be interpreted as global modes, namely a flexural mode along the structure's long side and two flexural-torsional modes along the short side; conversely, the fourth and fifth modes are associated to local modes of diaphragms.

Similarly to other literature works [26,118], various modelling epistemic uncertainties as well a random uncertainties associated with mechanical properties were considered to calibrate the model, specifically those related to: the stiffness of the diaphragm; the elastic moduli of masonry; the interaction with the elevator shaft in reinforced concrete, external to the main plan of the school building (see Fig. 4). To establish the best option, the minimization in terms of frequency error and the maximization of the Mac Assurance Criterion (MAC) matrix were adopted as targets. In particular, the MAC allows to verify the match in terms of modal shapes.

Among the various options considered, it was found that the concrete elevator shaft did not influence the dynamic response and frequencies of the building. Among the various options in terms of mechanical parameters, the solution that came closest to the real response of the monitored building was that of masonry with mortar of good characteristics. Therefore, following the values recommended by the Italian Code for this typology (refer to [32]), the Young's modulus was set to 224 MPa, perfectly plausible for the masonry type that characterizes the school. Fig. 7 compares the experimental and simulated frequencies and the MAC matrix of the parametric analyses related to the diaphragm stiffness, for the five modal shapes respectively (see Fig. 7b and Fig. 7c).

The calibrated model shows frequency errors below 5 % for the first three modes, with very good MAC values for the first and fourth modes, but lower values for the second and third modes. This outcome may be ascribable to the presence of walls arranged in non-orthogonal directions (Fig. 5), which could affect the actual measurement direction of the sensors positioned on them. This aspect will be explored further in the future; however, it goes beyond the scope of the present work and does not affect the analyses discussed in the following sections.

Thus, overall, the results are quite satisfactory, making the model calibration acceptable for this paper's main goals.

4. Obtained fragility curves

4.1. Sensitivity of results to thresholds adopted for defining the DLs

This Section presents the results of the sensitivity analysis performed, following the various steps described in Section 2.2, to define the DSs and at the end of the iterative process the DLs.

The options reported in Table 1 have been applied to the numerical models of school buildings, and in particular, Fig. 8 shows the results obtained for two case studies, e.g. the CS1 and CS2 as resulting from the Cloud analysis. The figure aims to highlight the potential impact that each may have on the definition of the fragility curves without iterative process.

Since the difference between the first four options (i.e. from Opt1 to Opt4) is on the threshold of the lowest DSs, it can be seen that the curves of the highest DSs are not sensitive to them; on the other hand, considering the last options (i.e. Opt5 to Opt7), the opposite is observed: in fact, the only difference between the curves can be seen on the highest DSs.

In particular, Fig. 8 shows that Opt1 and Opt2 have minimal impact on the curve; therefore, Opt2 was adopted. For lower levels of damage, a distribution of damage across the building is preferred over a peak in any one direction. Comparing Opt2 and Opt3, the CS2 model shows slightly more variance than the CS1 model, but these differences remain relatively minor. Consequently, Opt2 was chosen to validate the initially assumed thresholds, ensuring maximum consistency with the EMS-98

Table 4
Values of the mechanical parameters assumed for the schools analysed, increased in the presence of improving characteristics (e.g. good mortar quality (MQ), horizontal string bands (SB), good cross connection (CC), injections (I)).

Case study	Masonry Type	MQ	SB	CC	I	f_m [N/mm^2]	τ_0 [N/mm^2]	E [N/mm^2]	w [kN/m^3]
CS1	Uncut Stones [72 %]		X	X		2.94	0.051	1212	20
	Solid brick [28 %]					4.35	0.105	1470	18
CS2	Solid brick [100 %]	X				5.02	0.121	2205	18
CS3	Cut Stone [100 %]				X	4.71	0.097	2585	21
CS4	Cut Stone [100 %]	X				4.09	0.084	2240	21
CS5	Cut Stone [99 %]	X		X		5.31	0.109	2240	21
	Solid brick [1 %]	X		X		6.52	0.157	2205	18
CS6	Uncut Stones [100 %]	X		X		5.14	0.089	1697	20
CS7	Cut Stone [89 %]	X		X		5.31	0.109	2240	21
	Modern Masonry [11 %]					8.55	0.240	10182	18

	$G = 1.31x10^{10}$ Nm^{-1}					$G = 1.31x10^{11}$ Nm^{-1}					$G = 1.31x10^{10}$ Nm^{-1} + good mortar quality				
f (Hz)	3.63	4.13	4.34	7.12	7.95	3.65	4.13	4.34	7.27	8.55	4.18	4.74	4.92	7.80	8.62
err	0.18	0.09	0.10	-0.20	-0.24	0.17	0.09	0.10	-0.22	-0.34	0.05	-0.04	-0.02	-0.31	-0.35
4.40	**0.66**	0.01	0.04	0.00	0.02	**0.66**	0.01	0.04	0.00	0.03	**0.80**	0.02	0.03	0.00	0.02
4.55	0.20	**0.54**	0.02	0.01	0.02	0.21	**0.54**	0.02	0.01	0.02	0.21	**0.54**	0.02	0.01	0.01
4.80	0.20	0.22	**0.49**	0.05	0.00	0.20	0.22	**0.49**	0.04	0.01	0.12	0.22	**0.59**	0.06	0.00
5.95	0.00	0.02	0.02	**0.79**	0.00	0.01	0.02	0.02	**0.81**	0.00	0.00	0.00	0.00	**0.83**	0.00
6.40	0.19	0.01	0.16	0.11	**0.33**	0.19	0.01	0.16	0.10	**0.44**	0.20	0.00	0.18	0.10	**0.32**

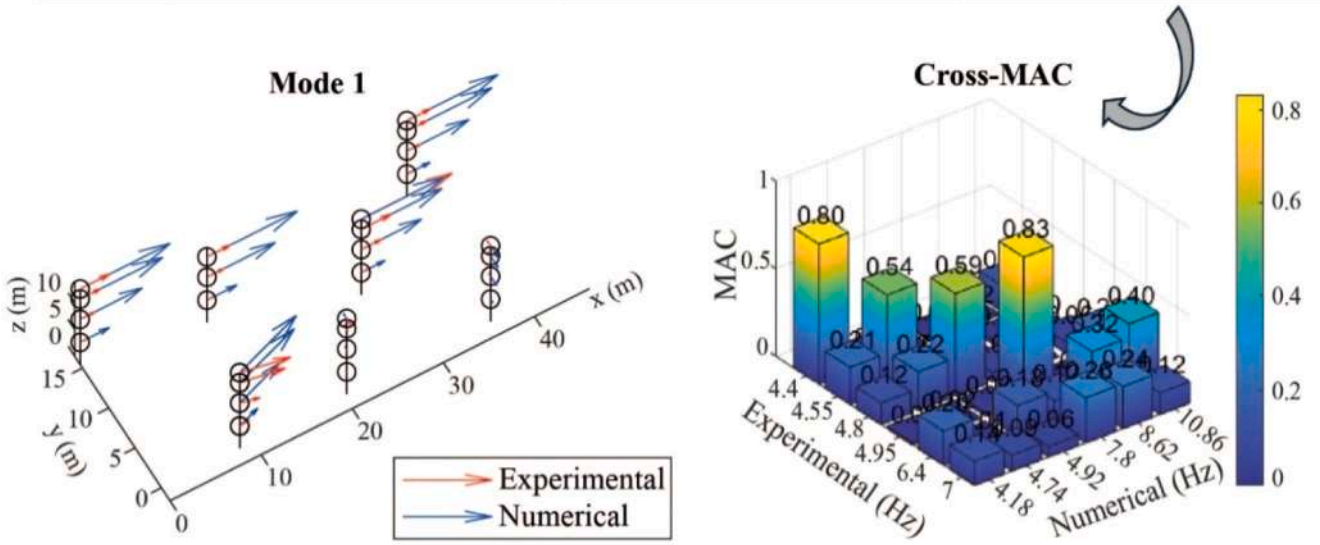

Fig. 7. – Comparison between the experimental and simulated numerical frequencies and the MAC matrix of the building having calibrated the equivalent shear stiffness of the diaphragm (expressed by the value of the G modulus) starting from the identified value and having assumed the improved coefficient related to the presence of good mortar characteristics.

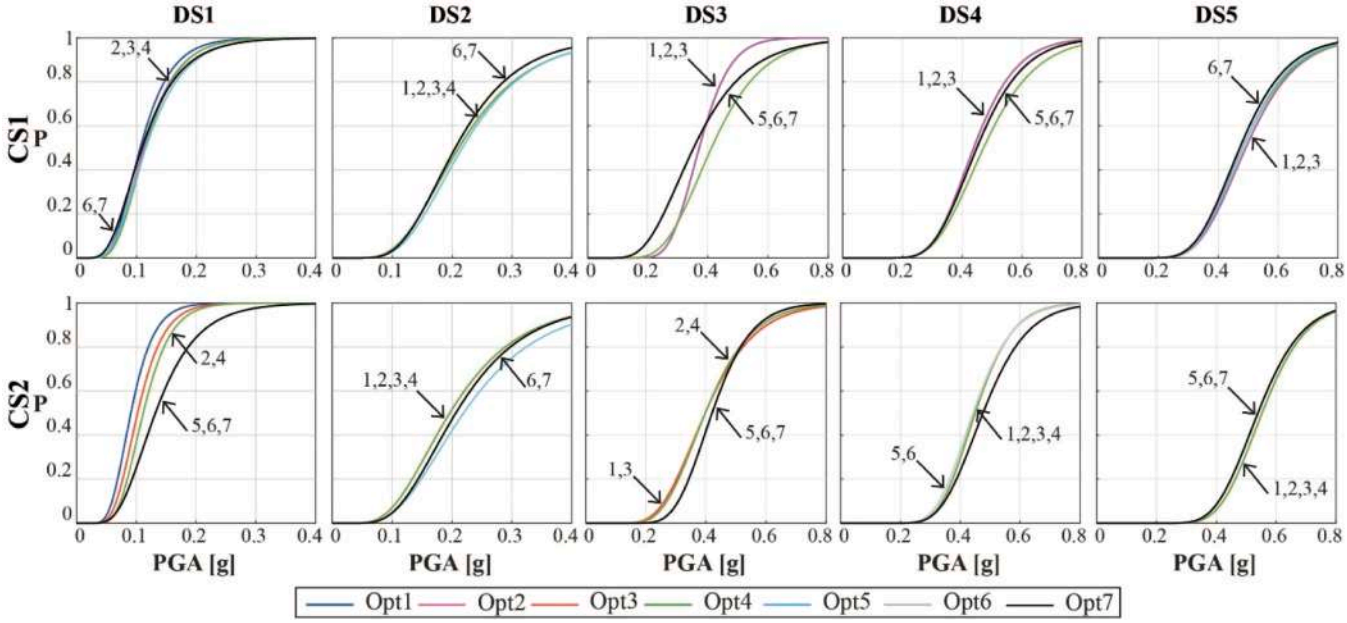

Fig. 8. Sensitivity of results to thresholds adopted to define the DSs for the CS1 and CS2 schools. The numbers reported in each box represent the options of Table 1 and are intended to give information on which curves overlap.

damage definitions.

Starting with Opt4, the definitions of DS2 (and DL2) and DS3 (and DL3) were modified to better distinguish these two damages. When comparing Opt2 and Opt4, the distinctions between DSs remain limited (with only DS3 and DS4 differing slightly in the CS1 model), so the multilinear approach (e.g., Opt4) was deemed appropriate, though the advance and retreat percentages required further calibration.

Between Opt4 and Opt5, Opt5 was selected. While higher DSs (i.e., DS3, DS4, and DS5) show little difference between the two options, Opt5 provides a shift which seems more convincing for lower DSs (i.e., DS1 and DS2), allowing the fragility curve to be a bit less fragile through an iterative approach.

Comparing Opt5 and Opt6 reveals that the earlier advance on DS3 consequent to the adoption of Opt5 had little effect on defining DSs. Since the curves show negligible variation between these options, Opt6 was adopted. Opt6 provides well-defined spacing between DS1, DS2, and DS3, while DS4 and DS5 yield nearly identical results (as the iterative method causes DS5 to shift backward). Thus, between Opt6 and Opt7, Opt7 was selected to improve the separation between DS4 and DS5, which were otherwise too close. It is important to note that Opt7 does not alter the fragility curve for DS5 compared to Opt6 but only affects DL4, as very destructive analyses are categorized within DS5, making them less sensitive to this adjustment.

Opt. 7 was finally selected to apply the iterative procedure described in the previous section and to pass from the DS to DL definition.

Fig. 9 shows the building-by-building variability, giving an idea of the dispersion of results in terms of fragility curves, fixed the DL. Moreover, Fig. 9 also highlights the variability associated with the record-to-record variability, with dispersion that varies from 0.2 to 0.4, values which are in lines with other literature works [24].

While spectral acceleration for the building's fundamental period generally proves to be more effective than PGA for flexible structures, this isn't always the case for rigid ones such as masonry buildings, owing to irregular spectral shapes in the low-period range. It is worth recalling that these fragility curves don't account for the intra-building variability since mechanical parameters have been considered deterministic.

Unlike other studies, this work does not consider material property uncertainty nor that associated to the drift limits, as the objective was to assess the procedure using deterministic building models. In other studies (e.g. [11,12,24,66]) such uncertainty was addressed by performing Monte Carlo sampling of the material property values. From the studies available in the literature, it emerges that the uncertainty contribution to the dispersion due to the material properties and drift limits is around 0.15–0.3. Thus, such a contribution is expected to be not dominant in fragility curves referring to a single structure [12,24,66] and not to a building class.

For the same reason, also the impact of other epistemic uncertainties associated to the effectiveness of structural details (like as the tie-rods, the length of reinforced concrete elements or the quality of walls-to-walls connection) was not part of the analysis in this paper. A more in-depth discussion on this aspect can be found, for instance, in [54,53,57]. Indeed, depending on the geometrical configuration of the buildings, the impact of such type of epistemic uncertainties may be even more significant than that of aleatory ones but, as aforementioned, this aspect is out of the scope of this paper.

The fragility curves derived at the end of the Cloud+IDA method allowed estimating the record-to-record variability (σ_{rr}) and quantifying the contribution associated to the inter-building variability. For the latter, fragility curves of low- and medium- rise school buildings have been grouped together. Table 5summarizes these values, where σ_{tot} include both sources of uncertainties. The resulting value of the inter-building variability ranges from 0.07 to 0.25. These values are a bit

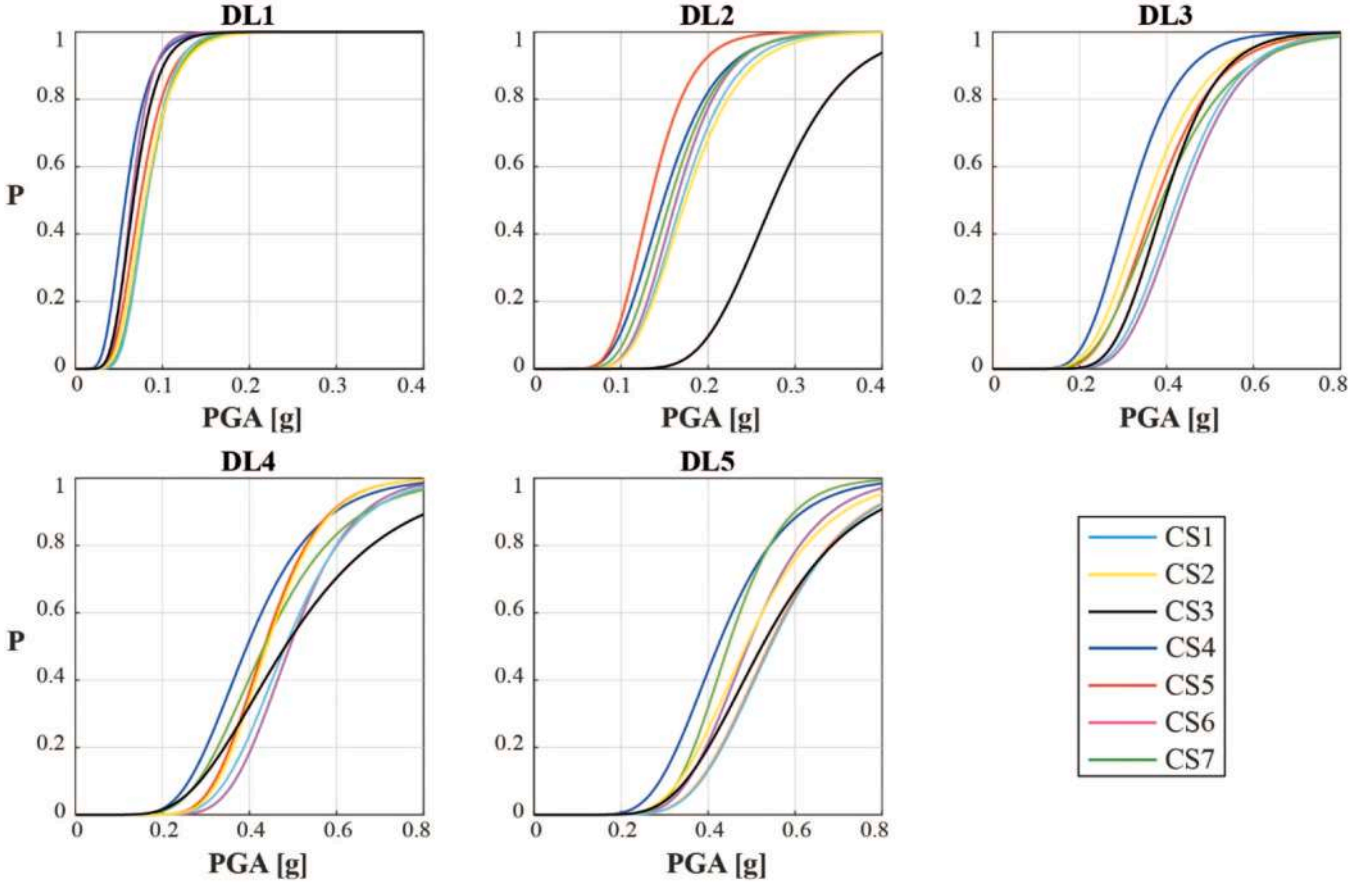

Fig. 9. Fragility curves obtained for the analysed schools by considering Opt7 at the end of the iterative procedure.

lower compared to other studies like as for example those reported in [53]. However, it should be noted that the number of buildings in our study is significantly lower (i.e. 7) compared to the latter (around 100 buildings).

4.2. Comparison of derived fragility curves with those achievable from a drift-based approach

This section presents a comparison between the fragility curves obtained using the proposed approach—where the damage level is assigned by directly interpreting the damage simulated through NLDA—and those obtained using the "traditional" DL approach, where the damage level is assigned based on predefined drift thresholds. Instead of adopting fixed threshold values from the literature (e.g., [17, 48]), building-specific thresholds were determined from the execution of pushover analyses according to the criteria defined in Table 5. The threshold derived from NLSA, differentiated for the positive and negative directions, refer to the lower value obtained by considering the two load patterns (i.e. uniform and inverted triangular) are reported in Table 6. At least, such an approach allows to consider customized threshold for each individual building.

Fig. 10 illustrates, for three of the seven examined structures, an example of this comparison, focusing on DL2 and DL4. Here, the term "traditional approach" refers solely to the method used for assigning the damage level and thus post-processing the NLDA results. The analyses themselves-whether following the classical Cloud method or the combined Cloud+IDA method-remain unchanged. The traditional approach was applied only in conjunction with the Cloud method, as this is the most commonly adopted in the literature. CS1 structure is the one whose results are depicted also in Fig. 1.

For DL2, the results indicate that the traditional approach can yield either lower or higher vulnerability estimates compared to the "proposed approach + Cloud" with amount in the differences varying across structures. This irregular trend may be related to the inherent limitations of nonlinear static analyses in reproducing the damage patterns simulated by NLDA, which in some cases exhibit more localized damage. In the case of DL4, instead usually the traditional approach produces lower vulnerability estimates compared to the "proposed approach + Cloud".

Conversely, as discussed in the paper, when the Cloud+IDA method is employed, the median value of the fragility curve decreases with values that are always lower than both the proposed and traditional approaches combined with the Cloud method. It is worth noting that, in the traditional approach, the fragility curve for DS2 corresponds to a range bounded by the thresholds for DL2 and DL3. Consequently, it is consistent that its median value is higher than that obtained with the Cloud+IDA method, which allows for a more precise identification of the attainment of DL2.

Instead, the differences for DL4 are much less pronounced.

Table 6
Thresholds adopted for the definition of the roof drift by performing the NLSAs.

Damage Level	Drift threshold
DL1	$\delta_{roof} = d\left(\frac{V_b}{V_{max}} = 0.4\right)/H_{tot}$
DL2	$\delta_{roof} = d\left(\frac{V_b}{V_{max}} = 0.98\right)/H_{tot}$
DL3	$\delta_{roof} = d\left(\frac{V_b}{V_{max}} = 0.70\right)/H_{tot}$
DL4	$\delta_{roof} = d\left(\frac{V_b}{V_{max}} = 0.40\right)/H_{tot}$
DL5	$\delta_{roof} = d\left(\frac{V_b}{V_{max}} = 0.50\right)/H_{tot}$

5. Comparison with literature's fragility curves

To validate the obtained results, the Cloud+IDA numerical fragility curves have been compared with other ones already available in the literature.

Firstly, the fragility curves developed in the MARS-School project [19] have been considered. These fragility curves integrate the results of various approaches, i.e.: the heuristic-macroseismic approach [70]; the simplified DBV-Masonry analytical-mechanical approach [21,72]; the empirical-binomial approach [40]; the Vulnus hybrid analytical-mechanical approach [109]; and the simplified Firstep-M analytical-mechanical approach [50,51,54]. Thus, these curves account also for the epistemic uncertainty related to the approach adopted for deriving the fragility curves. More specifically, they have been derived to the representative of the school building stock at national scale, considering school buildings' samples of different types. Specifically, the empirical models are based on data observed following the earthquake that struck the Abruzzo region in 2009, the DBV-Masonry and Vulnus analytical models developed fragility curves from a stock of prototype buildings scattered throughout Italy, the Firstep-M analytical-mechanical model was based on the FVG school sample.

In Fig. 11 the fragility curves of the analyzed schools (coloured lines) obtained with the Cloud+IDA numerical approach are compared with those from the MARS-School project [19]. For the latter, two ages of construction are considered, a more ancient (in light grey) and a more recent (in dark grey) one, respectively. In particular, the region resulting for "ancient" sub-typologies MARS fragility curves is limited by the results associated with 1921–45 and that to 1946–60 age of constructions; the region instead associated with "modern" sub-typologies results from 1961 to 75 and after 1976 age of construction. The comparison is made for 2-storeys and $\geq$ 3-storeys structures. This range of age of constructions has been considered since the school examined in this paper are characterized by structural details pertinent to these periods. In Fig. 11, also the fragility curves presented in [40] which have been derived from the observed data of school buildings hit by the L'Aquila 2009 earthquake are reported. Specifically, for the 1946–60 sub-typology, the dashed lines in light grey refer to the empirical-binomial approach developed by [60] while the lines in black refer to the heuristic approach

Table 5
Values obtained for the dispersion associated to the record-to-record variability (σ_{rr}) and to overall one accounting also for the inter-building variability combined curves (σ_{tot}).

	DL1		DL2		DL3		DL4		DL5	
	σ_{rr}	σ_{tot}	σ_{rr}	σ_{tot}	σ_{rr}	σ_{tot}	σ_{rr}	σ_{tot}	σ_{rr}	σ_{tot}
2 storey	0.372	0.365	0.322	0.312	0.288	0.308	0.323	0.276	0.296	0.303
	0.342		0.278		0.298		0.238		0.273	
	0.283		0.280		0.260		0.262		0.272	
	0.343		0.291		0.308		0.232		0.296	
3/4 storey	0.282	0.323	0.270	0.372	0.255	0.284	0.233	0.338	0.258	0.280
	0.307		0.294		0.329		0.337		0.231	
	0.326		0.244		0.247		0.408		0.319	

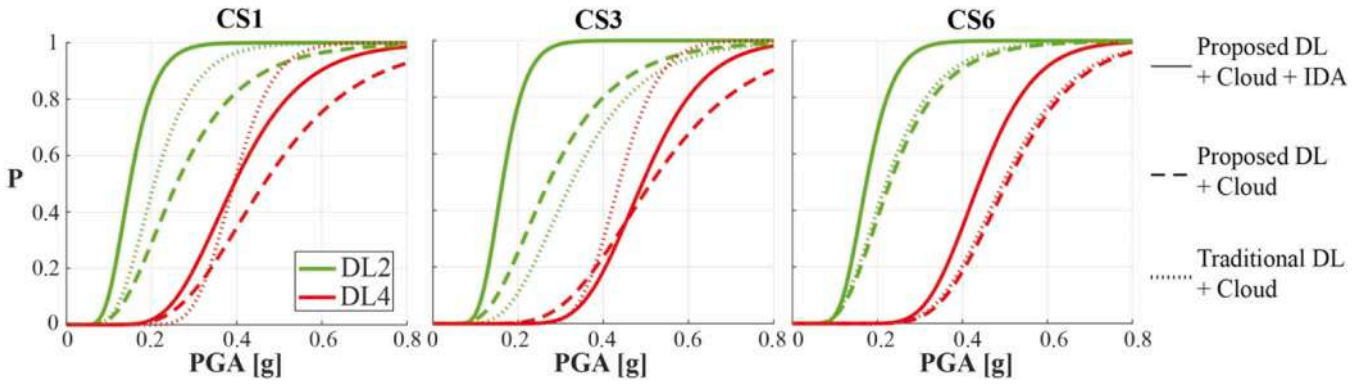

Fig. 10. Comparison between the fragility curves derived with the proposed procedure and those from a traditional approach based on the use of roof drift thresholds defined from NLSAs.

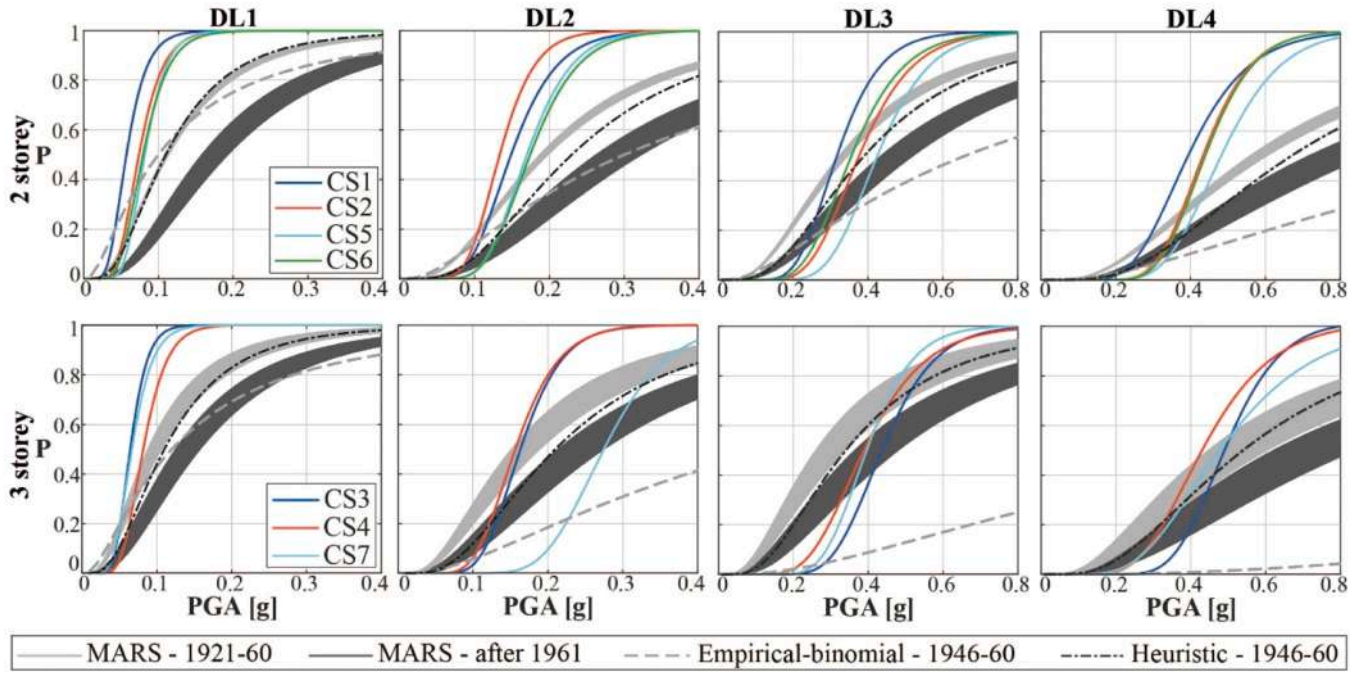

Fig. 11. Numerical fragility curves of the seven analyzed schools, compared with the MARS-School project literature curves [19] (area in light grey refers to ancient schools, that in dark grey to the modern age of construction). Moreover, the empirical-binomial literature curves (dashed lines in light grey) and the heuristic literature curves (stretch dot lines in black) [40] for the 1946–60 sub typology are reported too.

developed by [70].

From the analysis of the figure and considering the differences in the examined approaches, the following observations can be made:

- The variation in the dispersion of the fragility curves arises from the different uncertainty contributions considered. The curves derived from NLDAs account only for the record-to-record variability, while those from the MARS project incorporate contributions from various uncertainty sources, including seismic input, structural capacity, and damage level definitions, as well as epistemic uncertainties associated with the approach used for their derivation.
- The MARS project curves represent typological classes across all of Italy, whereas those from NLDAs are associated with single realizations of specific buildings. Thus, as the number of schools examined increases, the median values are expected to converge a bit.
- For three-storey structures, starting from DL2, the median values of the NLDA curves are relatively well-aligned. Conversely, in the case of two-storey structures, the NLDA results are generally more conservative. Such a results could be attributed to a prevalence in the numerical models to activate a quite pure soft-storey mechanism in case of low-rise buildings with reinforced concrete beams and rigid diaphragms as those examined.
- For both two- and three-storey school buildings, the DL1 NLDA curves are more conservative.

The tendency for NLDAs results to be more conservative than other approaches has also been confirmed in the literature for other structural types, such as reinforced concrete schools within the MARS School project [19]. Specifically, in the case of DL1, this outcome for URM buildings could be attributed to a tendency of the numerical model to overestimate the onset of minor damage at the structural element scale. Phenomenological constitutive laws, like the one adopted here, approximate the progressive stiffness degradation in the initial phase, potentially contributing to this effect. It should also be noted that when assigning real damage levels based on expert judgment, the greatest uncertainties and dispersion are observed at the lower damage levels.

Despite these differences, overall, the comparison seems quite good

considering also the substantial differences in the approaches adopted and results aligned.

Finally, the results are also examined in terms of distance among fragility curves for investigating the ductility assessed for the examined building stock. With this aim the ratios PGA_{DLk}/PGA_{DL2} have been computed and compared with some reference values proposed in the literature within the MARS project ([83,19]).

Specifically, according to the approach proposed in [69,83], the value PGA_{DL2} serves as a reference, representing moderate-slight structural damage, near the point of maximum shear strength, while the ratio PGA_{DLk}/PGA_{DL2} introduces an important concept connected to "ductility" (or more precisely, the "behavior factor") for levels DL3, DL4, and DL5. Conversely, the value PGA_{DL1}/PGA_{DL2} represents the overstrength ratio in URM buildings. According to this proposal, a differentiation between brittle and ductile behavior is introduced by considering possible variations in the spacing of fragility curves associated with different DLs. Specifically, in [69] two sets of fragility curves, labeled "brittle" and "ductile", are proposed based on the reference values for the PGA_{DLk}/PGA_{DL2} ratio summarized in Table 7.

This table reports also these ratios as resulting from the fragility curves derived from the NLDAs presented in the paper. To be more effective, Fig. 12 graphically illustrates the same results. It emerges that while the distance between DL2 and DL3 obtained from NLDAs is higher than the reference ductile behaviour established within MARS project, that between DL2 and DL4 is intermediate between the ductile and fragile behaviour. What it clearly appears is that the progression from DL4 to DL5 estimated by the mechanical-numerical approach is very moderate. However, such a result is ascribable to the fact that the numerical approach tends to saturate collapse prediction: this seems related to a limitation of the approach more than a consistent trend. Overall, this comparison confirms a quite good agreement with trends available from other research studies of literature.

6. Derivation of reference roof and interstorey drifts from the NLDAs carried out

The procedure proposed in this paper is self-consistent and uses only NLDA, presupposing, however, the availability of a model to estimate the spread of damage. Since not always so detailed numerical models are available, such as the case of NLDAs on single degrees of freedom, therefore a threshold definition method must be applied. This is why reference values for roof drifts of each DL were also estimated ex-post from NLDAs.

The maximum wall-roof drift ($\delta_{\max}$) is calculated considering not only the contribution of the horizontal displacements by also that of the average rotations of the nodes at the top storey. Given the different behaviour of the buildings in the two verses (positive or negative), the maximum roof drift has been evaluated separately for the two directions ($\delta_{\max\_X}$ and $\delta_{\max\_Y}$) as reported in Eq. (4)

$$\delta_{\max} = \max\left\{\delta_{positive} \;;\; \delta_{negative}\right\} \tag{4}$$

Table 7
PGA_{DLk}/PGA_{DL2} ratio for each analyzed school building with respect to the "brittle" and "ductile" vulnerability class proposed in [69].

Case study	$\frac{PGA_{DL1}}{PGA_{DL2}}$	$\frac{PGA_{DL3}}{PGA_{DL2}}$	$\frac{PGA_{DL4}}{PGA_{DL2}}$	$\frac{PGA_{DL5}}{PGA_{DL2}}$
CS1	0.39	2.13	2.65	2.84
CS2	0.55	2.82	3.25	4.05
CS3	0.39	2.67	3.02	3.01
CS4	0.52	2.48	2.77	2.85
CS5	0.48	2.50	2.84	3.20
CS6	0.46	2.04	2.52	2.79
CS7	0.24	1.44	1.75	1.90
Fragile vulnerability class	0.67	1.49	2.23	3.32
Ductile vulnerability class	0.51	1.95	3.82	7.46

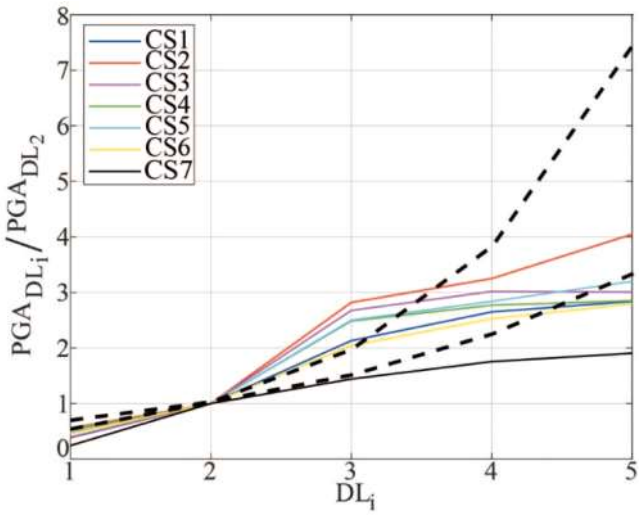

Fig. 12. Graphical representation of the ratios shown in the Table 7 for each analyzed school building.

Then, for each building, the $\delta_{DLi,roof,NLDA}$ obtained from the NLDAs was evaluated as described in Eq. (5).

$$\delta_{DLi,roof,NLDA} = \max\left\{\delta_{DLi,X}; \delta_{DLi,Y}\right\} \tag{5}$$

Specifically, for each analysis considered, the maximum roof drift between the two directions associated with the DL reached (following the procedure described in Section 2.2) was identified. Subsequently, the median value and dispersion of the roof drift were calculated for each DL. Table 8 summarizes the values obtained from both the NLDAs carried out through the classical approach or the refined one through the IDA and iterative procedure. For the procedure without the iteration the values are representative of DS, but for brevity, they are called DLs. Fig. 13 shows the values of the ratios between the maximum δ_{roof} in Table 8 with and without iterative procedure.

Analyzing the effects of the Cloud+IDA iterative procedure, it is possible to affirm that:

- the definition of DL1 and DL2 are the most affected by the iterative procedure, and in particular they tend to move back (on average the ratio between the wall-roof drift from the Cloud+IDA procedure and the Cloud one is about 0.6).
- Concerning DL3 and DL4, the ratio is in average about 0.87 while for DL5 the impact is higher, with a ratio equal in average to 0.6. Consequently, the DLs tend to converge with each other after the application of the iterative procedure. This may depend on the response of the building having a "brittle" behavior and not a gradual softening phase (typical of buildings with rigid diaphragms). The result is consistent with the position of these three DLs on the pushover and the fragility of the softening response.

The $\delta_{DLi,roof,NLSA}$ obtained by performing NLSA are summarized in Table 6 as well. The value computed as illustrated in Section 4.2 has been evaluated, for each building, as reported in Eq. (6):

$$\delta_{DLi,roof,NLSA} = \min\left\{\delta_{DLi,X}; \delta_{DLi,Y}\right\} \tag{6}$$

The roof drifts resulting from both NLDAs and NLSAs (as reported in Table 8) may exhibit considerable variation among buildings. That is attributed to the activation of different failure modes across various configurations and/or storey numbers. It can be observed that the thresholds obtained from NLSA are usually lower than those from NLDA. This result is in favour of safety, as NLSAs, being more expeditious and less accurate than NLDAs, must give more precautionary results. However, as illustrated in Section 4.2 not always that corresponds to fragility

Table 8
Values of the maximum roof drift obtained for the schools analyzed with NLSA, NLDA using the cloud method and NLDA using the iterative procedure, plus the dispersion obtained by all the analyses that belong to a DL.

School no.		NLSA	NLDA-Cloud Method		NLDA-Iterative Procedure	
		δ_{max} [%]	δ_{max} [%]	σ	δ_{max} [%]	σ
CS1	DL1	0.02	0.07	0.332	0.04	0.159
	DL2	0.11	0.17	0.319	0.11	0.198
	DL3	0.29	0.34	0.163	0.28	0.088
	DL4	0.35	0.49	0.152	0.41	0.135
	DL5	0.42	1.41	0.593	0.78	0.324
CS2	DL1	0.01	0.04	0.272	0.03	0.161
	DL2	0.07	0.12	0.433	0.06	0.180
	DL3	0.20	0.28	0.238	0.26	0.155
	DL4	0.35	0.48	0.344	0.37	0.173
	DL5	0.39	1.61	0.529	0.94	0.336
CS3	DL1	0.01	0.02	0.306	0.01	0.126
	DL2	0.05	0.08	0.534	0.04	0.178
	DL3	0.19	0.26	0.240	0.23	0.143
	DL4	0.25	0.32	0.149	0.33	0.150
	DL5	0.30	0.96	0.533	0.46	0.497
CS4	DL1	0.01	0.04	0.283	0.03	0.086
	DL2	0.07	0.12	0.425	0.07	0.128
	DL3	0.22	0.28	0.540	0.27	0.166
	DL4	0.26	0.45	0.203	0.41	0.217
	DL5	0.27	0.75	0.463	0.55	0.224
CS5	DL1	0.01	0.04	0.325	0.03	0.115
	DL2	0.08	0.12	0.435	0.06	0.170
	DL3	0.31	0.34	0.272	0.28	0.182
	DL4	0.40	0.49	0.234	0.44	0.215
	DL5	0.51	1.19	0.573	0.75	0.312
CS6	DL1	0.01	0.06	0.346	0.04	0.159
	DL2	0.07	0.14	0.318	0.10	0.213
	DL3	0.31	0.32	0.152	0.26	0.119
	DL4	0.39	0.48	0.231	0.37	0.156
	DL5	0.49	1.47	0.520	0.89	0.448
CS7	DL1	0.01	0.02	0.508	0.01	0.127
	DL2	0.03	0.08	0.391	0.06	0.310
	DL3	0.19	0.15	0.353	0.12	0.305
	DL4	0.30	*	1.318	0.22	0.673
	DL5	0.36	0.81	0.622	0.53	0.545

* This value is not statistically robust and is therefore not reported.

curves more vulnerable.

Moreover, it can be observed that the intra-building dispersions reported in Table 5 and computed from NLDAs are significant as well; however, it is worth recall that this dispersion accounts only for the influence of the record-to-record variability.

To be useful in risk analyses at large scale values summarized in Table 5 have been aggregated in Table 8 on the complete sample of examined structures (first row) or grouped for 2-storey buildings and 3–4 storey buildings (second and third rows). Table 9 also reports the inter-storey drift limits proposed by FEMA [48,68,93]. These values are provided for four damage states (Slight, Moderate, Extensive, Complete), which have been associated in this comparison with DLs: DL2 to DL5, respectively. Since all the analysed buildings are equipped with reinforced concrete beams, it is assumed that their seismic performance may fall between the Pre-Code and Low-Code Seismic Design Levels. Low-rise buildings are considered those with 1 or 2 storey, while Mid-rise buildings have more than 3 storey. The comparison with the values proposed by FEMA shows that, for DL2 and DL4, the thresholds obtained using the Cloud-based approach are significantly lower than those of FEMA, while they are more comparable for DL3. In general, differences between low- and medium-rise buildings are smaller than those indicated by FEMA. For all damage levels, the thresholds resulting from the Cloud+IDA approach are significantly lower.

Moreover, it is important to keep in mind that the reference values proposed in Table 9 refer to building with specific features, i.e. with rigid diaphragms and certain masonry types. Moreover, the estimated thresholds also do not consider the dispersion associated with other sources of uncertainties (e.g. mechanical properties, drift limits at scale of pier and spandrels, structural details); therefore, it is expected that the associated dispersion could be even larger in the reality.

7. Conclusions

The paper explores the derivation of fragility curves through an accurate mechanical-numerical approach based on nonlinear dynamic analyses (NLDAs). Although the presented application pertains to URM school buildings, the proposed procedure is general and can also be applied to other types, such as residential or monumental structures (like palaces). The strength of the developed procedure lies in the self-consistent use of the dynamic approach, relying exclusively on the interpretation of simulated damage without the need to define conventional thresholds based on more approximate analyses, for instance, those resulting from applying the nonlinear static approach.

The method adopted for interpreting the simulated damage is based on a methodologically consistent approach to damage level definitions according to EMS98. It contributes to reducing potential discrepancies associated with different damage metrics across various approaches for deriving fragility curves.

The method in this paper based on the execution of NLDA on 3D models, is expected to be more effective than other more simplified approach, such as based on the use of SDOF systems, particularly for

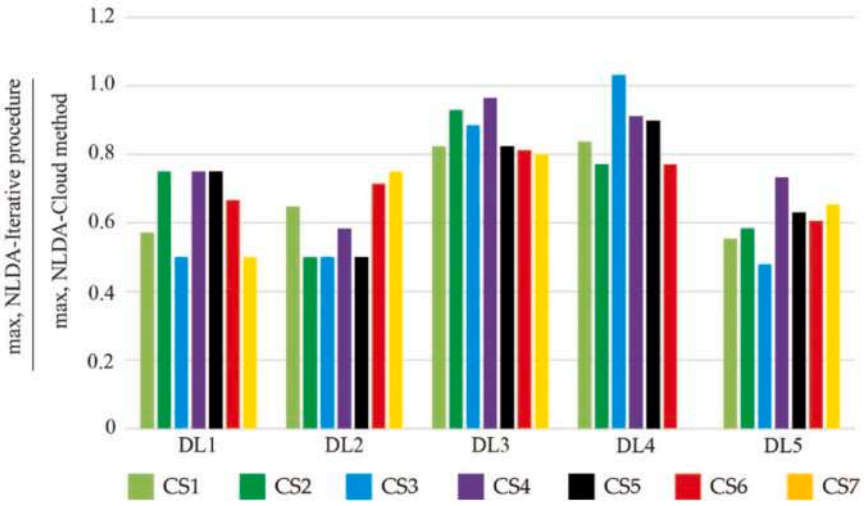

Fig. 13. Ratio of the average δ_{roof} resulting from NLDAs with and without iterative process, for the seven examined case studies (CS).

Table 9
Median values of the roof and interstorey drift obtained for the whole sample, for the 2-storey and the 3-storey buildings, using the cloud method and the Cloud+IDA method.

			δ_{DL1} [%]	σ_{DL1}	δ_{DL2} [%]	σ_{DL2}	δ_{DL3} [%]	σ_{DL3}	δ_{DL4} [%]	σ_{DL4}	δ_{DL5} [%]	σ_{DL5}
δ_{roof}	**NLDA – Cloud**	**Sample**	0.04	0.206	0.12	0.184	0.27	0.438	0.33	0.751	1.13	0.098
	Method	**2-storey**	0.05	0.107	0.13	0.178	0.32	0.283	0.49	0.333	1.41	0.063
		3/4-storey	0.03	0.318	0.09	0.161	0.23	0.407	0.19	1.180	0.84	0.148
	NLDA –	**Sample**	0.02	0.228	0.07	0.268	0.24	0.384	0.35	0.547	0.68	0.311
	Iterative procedure	**2-storey**	0.03	0.164	0.08	0.099	0.27	0.320	0.40	0.196	0.84	0.164
		3/4-storey	0.02	0.220	0.06	0.448	0.20	0.401	0.31	0.783	0.51	0.489
$\delta_{interstorey}$	**NLDA – Cloud**	**Sample**	0.05	0.226	0.15	0.165	0.40	0.419	0.53	0.677	2.47	0.136
	Method	**2-storey**	0.05	0.105	0.16	0.153	0.43	0.154	0.78	0.225	2.69	0.180
		3/4-storey	0.04	0.369	0.13	0.170	0.35	0.560	0.32	1.094	2.22	0.014
	NLDA –	**Sample**	0.03	0.233	0.08	0.319	0.34	0.449	0.56	0.581	1.39	0.247
	Iterative procedure	**2-storey**	0.03	0.213	0.09	0.192	0.37	0.388	0.59	0.282	1.55	0.111
		3/4-storey	0.02	0.169	0.07	0.484	0.31	0.493	0.52	0.870	1.20	0.349
	FEMA	**Low-rise**	/		0.30		0.60		1.50		3.50	
	Low-Code	**Mid-rise**	/		0.20		0.40		1.00		2.33	
	FEMA	**Low-rise**	/		0.24		0.48		1.20		2.80	
	Pre-Code	**Mid-rise**	/		0.16		0.32		0.80		1.87	

irregular buildings or those with flexible diaphragms, as it explicitly considers the actual distribution of damage - an aspect that SDOF models are inherently unable to capture. In fact, particularly these configurations may be subjected to a more irregular or localized distribution of damage. The SDOF models, as well as typically mechanical models, can usually be correlated to damage only through roof drift or in some case (more rarely) inter-story drift. However, especially in the case of advanced damage states, roof drift may not be the most suitable indicator, as it fails to capture localized damage.

The fragility curves developed are compared in the paper with others available in the literature, showing overall good agreement, albeit with some differences attributable to intrinsic variations among methods.

Moreover, the results obtained from the NLDAs have been processed to provide roof drift and interstorey drift thresholds, which could serve as a useful reference for applications by other researchers relying on more simplified approaches that do not allow for the estimation of the damage distribution at the single structural element scale. Such reference thresholds are quite limited in the literature, and in the future, the proposed approach could be used to perform parametric analyses on configurations representative of various architectural/structural typologies and thus enrich these reference sets of values.

Furthermore, the comparison with the "traditional DL approach" indicates that adopting identical roof or inter-story drift thresholds for all buildings or customized on the structure but based on pushover analyses-may be arbitrary and may produce not always robust fragility curves. Thus, strengthening the research in the outlined direction therefore appears both necessary and beneficial.

Finally, the proposed procedure could have in the future wider areas of applications. A possible example lies in the development of decision-support tools for assessing the damage of permanently monitored strategic buildings, where accurate numerical simulations via NLDAs could complement the interpretation of synthetic parameters estimated from on-site measurements (as for example tentatively applied in [117].

CRediT authorship contribution statement

S. Giusto: Analysis, Data curation, Writing – original draft. **A. Brunelli:** Data curation, Writing – original draft. **S. Lagomarsino:** Supervision, Methodology, Fundings, Writing – review & editing. **S. Cattari:** Supervision, Methodology, Fundings, Writing – original draft and review&editing.

Declaration of Competing Interest

The authors declare that they have no known competing financial interests or personal relationships that could have appeared to influence the work reported in this paper.

Acknowledgements

The study presented in this article was developed in the framework of the MARS project (WP4), carried out within the activities of the ReLUIS-DPC 2022–2024 and 2024–2026 research program, funded by the Presidenza del Consiglio dei Ministri-Dipartimento della Protezione Civile (DPC). Note that the opinions and conclusions presented by the authors do not necessarily reflect those of the funding entity.

During the preparation of this work the author(s) used ChatGPT only to improve the quality of the English. After using this tool, the author(s) reviewed and edited the content as needed and take full responsibility for the content of the publication.

References

[1] Angiolilli M, Lagomarsino S, Cattari S, Degli Abbati S. Seismic fragility assessment of existing masonry buildings in aggregate. Eng Struct 2021;247(1):113218. https://doi.org/10.1016/j.engstruct.2021.113218.
[2] Angiolilli M, Minkada ME, Di Domenico M, et al. Comparing the observed and numerically simulated seismic damage: a unified procedure for unreinforced masonry and reinforced concrete buildings. J Earthq Eng 2022;28(4):1157–93. https://doi.org/10.1080/13632469.2022.2096721.
[3] Augenti Nicola, Parisi F, Prota A, Manfredi G. In-Plane lateral response of a Full-Scale masonry subassemblage with and without an inorganic Matrix-Grid strengthening system. J Compos Constr 2011;15(4):578–90. https://doi.org/10.1061/(ASCE)CC.1943-5614.0000193.
[4] Barros Rui, Braz Manuel, César, Naderpour H, Khatami Seyed. Comparative review of the performance based design of building structures using static Non-Linear analysis - part B: R/C Frames'. J Rehabil Civ Eng 2014;2(1):75–92. https://doi.org/10.22075/jrce.2014.214.
[5] Battaglia Lidia, Ferreira Tiago, Lourenco Paulo. Seismic fragility assessment of masonry building aggregates: a case study in the old city centre of seixal, Portugal. Earthq Eng Struct Dyn 2021;50:1358–77. https://doi.org/10.1002/eqe.3405.
[6] Bazzurro Paolo, Cornell C, Shome Nilesh, Carballo Jorge. Three proposals for characterizing MDOF nonlinear seismic response. J STRUCT ENGASCE J STRUCT ENGASCE 1998;124. https://doi.org/10.1061/(ASCE)0733-9445(1998)124:11(1281).
[7] Beyer Katrin, Dazio Alessandro. Quasi-Static cyclic tests on masonry spandrels. Earthq Spectra 2012;28:907–29. https://doi.org/10.1193/1.4000063.
[8] Borri A, Corradi M, Castori G, De Maria A. A method for the analysis and classification of historic masonry. Bull Earthq Eng 2015;13(9). https://doi.org/10.1007/s10518-015-9731-4.
[9] Boschi S, Galano L, Vignoli A. Mechanical characterisation of tuscany masonry typologies by in situ tests. Bull Earthq Eng 2019;17(1):413–38. https://doi.org/10.1007/s10518-018-0451-4.
[10] Bracchi Stefano, Galasco Alessandro, Penna Andrea. A novel macroelement model for the nonlinear analysis of masonry buildings. Part 1: axial and flexural behavior. Earthq Eng Struct Dyn 2021;50(8):2233–52. https://doi.org/10.1002/eqe.3445.
[11] Bracchi S, Rota M, Penna A, et al. Consideration of modelling uncertainties in the seismic assessment of masonry buildings by equivalent-frame approach. Bull Earthq Eng 2015;13:3423–48. https://doi.org/10.1007/s10518-015-9760-z.

[12] Brunelli Andrea, de Silva Filomena, Cattari Serena. Site effects and Soil-Foundation-Structure interaction: derivation of fragility curves and comparison with Codes-Conforming approaches for a masonry school. Soil Dyn Earthq Eng 2022;154:107125. https://doi.org/10.1016/j.soildyn.2021.107125.

[13] Brunelli A, de Silva F, Piro A, et al. Numerical simulation of the seismic response and soil–structure interaction for a monitored masonry school building damaged by the 2016 central Italy earthquake. Bull Earthq Eng 2021;19(2):1181–211. https://doi.org/10.1007/s10518-020-00980-3.

[14] Caicedo D, Karimzadeh S, Bernardo V, Lourenço PB. Selection and scaling approaches of earthquake time-series for structural engineering applications: state of art review. Arch Comput Methods Eng 2023;2023. https://doi.org/10.1007/s11831-023-10025-y.

[15] Caicedo D, Tomić I, Karimzadeh S, Bernardo V, Beyer K, Lourenço PB. Code-based ground motion selection and scaling for seismic assessment: application to two masonry building case studies. J Build Eng 2025;111:113558. https://doi.org/10.1016/j.jobe.2025.113558.

[16] Calò Mattia, Malomo Daniele, Gabbianelli Giammaria, Pinho Rui. Shake-Table response simulation of a URM building specimen using discrete Micro-Models with varying degrees of detail. Bull Earthq Eng 2021;19(14):5953–76. https://doi.org/10.1007/s10518-021-01202-0.

[17] Calvi Gian Michele. A displacement-based approach for vulnerability evaluation of classes of buildings. J Earthq Eng 1999;3(3):411–38. https://doi.org/10.1080/13632469909350353.

[18] Castellazzi G, Pantò B, Occhipinti G, et al. A comparative study on a complex URM building: part II—Issues on modelling and seismic analysis through continuum and Discrete-Macroelement models. Bull Earthq Eng 2022;20(2):2159–85. https://doi.org/10.1007/s10518-021-01147-4.

[19] Cattari S, Alfano S, Manfredi V, et al. National risk assessment of Italian school buildings: the Mars project Experience'. international. Int J Disaster Risk Reduct 2024;113:104822. https://doi.org/10.1016/j.ijdrr.2024.104822.

[20] Cattari S., Alfano S., Masi A., et al. (2022a). 'Risk Assessment of Italian School Buildings at National Scale: The MARS Project Experience'. in 3rd EUROPEAN CONFERENCE ON EARTHQUAKE ENGINEERING & SEISMOLOGY. Bucharest, Romania.

[21] Cattari S., Alfano S., Ottonelli D., Saler E., da Porto F. (2021b). 'Comparative Study on Two Analytical Mechanical-Based Methods for Deriving Fragility Curves Targeted to Masonry School Buildings'. Pp. 3155–75 in COMPDYN 2021 - 8th ECCOMAS Thematic Conference on Computational Methods in Structural Dynamics and Earthquake Engineering Methods in Structural Dynamics and Earthquake Engineering. Athens, Greece.

[22] Cattari Serena, Angiolilli Michele, Alfano Sara, Brunelli Andrea, de Silva Filomena. Investigating the combined role of the structural vulnerability and site effects on the seismic response of a URM school hit by the central Italy 2016 earthquake. Structures 2022;40:386–402. https://doi.org/10.1016/j.istruc.2022.04.026.

[23] Cattari S, Angiolilli M. Multiscale procedure to assign structural damage levels in masonry buildings from observed or numerically simulated seismic performance. Bull Earthq Eng 2022;20(13):7561–607. https://doi.org/10.1007/s10518-022-01504-x.

[24] Cattari Serena, Camilletti Daniela, Lagomarsino Sergio, Bracchi Stefano, Rota Maria, Penna Andrea. Masonry Italian Code-Conforming buildings. Part 2: nonlinear modelling and Time-History analysis. J Earthq Eng 2018;22(sup2):2010–40. https://doi.org/10.1080/13632469.2018.1541030.

[25] Cattari S., Degli Abbati S., Ottonelli D., et al. (2019). 'Discussion on Data Recorded by the Italian Structural Seismic Monitoring Network on Three Masonry Structures Hit by the 2016-2017 Central Italy Earthquake'. Pp. 1889–1906 in 7th International Conference on Computational Methods in Structural Dynamics and Earthquake Engineering Methods in Structural Dynamics and Earthquake Engineering. Crete, Greece.

[26] Cattari S, Degli Abbati S, Alfano S, Brunelli A, orenzoni, da Porto F F. Dynamic calibration and seismic validation of numerical models of URM buildings through permanent monitoring data. Earthq Eng Struct Dyn 2021;50(10):2690–711. https://doi.org/10.1002/eqe.3467.

[27] Cattari Serena, Lagomarsino Sergio. Masonry structures. In: Sullivan T, Calvi GM, editors. In Developments in the Field of Displacement Based Seismic Assessment. Pavia, Italy: IUSS Press and EUCENTRE; 2013.

[28] Cattari Serena, Magenes Guido. Benchmarking the software packages to model and assess the seismic response of unreinforced masonry existing buildings through nonlinear static analyses. Bull Earthq Eng 2022;20(4):1901–36. https://doi.org/10.1007/s10518-021-01078-0.

[29] Chieffo Nicola, Formisano Antonio, Lourenço Paulo B. Seismic vulnerability procedures for historical masonry structural aggregates: analysis of the historical centre of castelpoto (South Italy). Structures 2023;48:852–66. https://doi.org/10.1016/j.istruc.2023.01.022.

[30] Cima Valentina, Tomei Valentina, Grande Ernesto, Imbimbo Maura. Fragility curves at regional basis for unreinforced masonry buildings prone to Out-of-Plane mechanisms: the case of central Italy. Structures 2021;34:4774–87. https://doi.org/10.1016/j.istruc.2021.09.111.

[31] Cima Valentina, Tomei Valentina, Grande Ernesto, Imbimbo Maura. Fragility curves for the seismic assessment of masonry buildings in historic centres prone to Out-of-Plane failure modes. Bull Earthq Eng 2024;22(4):1801–26. https://doi.org/10.1007/s10518-023-01831-7.

[32] Circolare. 2019. 'Istruzioni per l'applicazione Dell'Aggiornamento Delle "Norme Tecniche per Le Costruzioni" Di Cui al Decreto Ministeriale 17 Gennaio 2018. G. U.S.O. n. 29 of 27/7/2018, No. 42, 21 Gennaio 2019'.

[33] D'Altri AM, Sarhosis V, Milani G, et al. Modeling strategies for the computational analysis of unreinforced masonry structures: review and classification. Arch Comput Methods Eng 2020;27(4):1153–85. https://doi.org/10.1007/s11831-019-09351-x.

[34] D'Ayala, Dina, Abdelghani Meslem, Dimitrios Vamvatsikos, Keith Porter, and Tiziana Rossetto. 2015. GEM Guidelines for Analytical Vulnerability Assessment of Low/Mid-Rise Buildings. GEM Technical Report. 2015-08 V1.0.0. Global Earthquake Model (GEM). doi: 10.13117/GEM.VULN---MOD.TR2014.12.

[35] D'Ayala, D.F., Meslem A. (2013). Guide for Selection of Existing Fragility Curves and Compilation of the Database, GEM Vulnerability Global Component Project. GEM Technical Report. 2013–X. GEM Foundation.

[36] da Porto F, Donà M, Rosti A, et al. Comparative analysis of the fragility curves for Italian residential masonry and RC buildings. Bull Earthq Eng 2021;19(8):3209–52. https://doi.org/10.1007/s10518-021-01120-1.

[37] Dávalos Héctor, Miranda Eduardo. Evaluation of bias on the probability of collapse from amplitude scaling using Spectral-Shape-Matched records. Earthq Eng Struct Dyn 2019;48(8):970–86. https://doi.org/10.1002/eqe.3172.

[38] Degli Abbati Stefania, Morandi Paolo, Cattari Serena, Spacone Enrico. On the reliability of the equivalent frame models: the case study of the permanently monitored Pizzoli's town hall. Bull Earthq Eng 2022;20(4):2187–217. https://doi.org/10.1007/s10518-021-01145-6.

[39] Demir Ahmet, Kayhan Ali Haydar, Palanci Mehmet. Response- and Probability-Based evaluation of spectrally matched ground motion selection strategies for Bi-Directional dynamic analysis of Low- to Mid-Rise RC buildings. Structures 2023;58:105533. https://doi.org/10.1016/j.istruc.2023.105533.

[40] Di Ludovico M, Cattari S, Verderame G, et al. Fragility curves of Italian school buildings: derivation from L'Aquila 2009 earthquake damage via observational and heuristic approaches. Bull Earthq Eng 2023;21(1):397–432. https://doi.org/10.1007/s10518-022-01535-4.

[41] Di Ludovico M, Prota A, Moroni C, et al. Reconstruction process of damaged residential buildings outside historical centres after the L'Aquila earthquake: part I - "Light Damage" reconstruction. Bull Earthq Eng 2017;15(2):667–92. https://doi.org/10.1007/s10518-016-9877-8.

[42] Di Ludovico M, Prota A, Moroni C, et al. Reconstruction process of damaged residential buildings outside historical centres after the L'Aquila earthquake: part II - "Heavy Damage" reconstruction. Bull Earthq Eng 2017;15(2):693–729. https://doi.org/10.1007/s10518-016-9979-3.

[43] Dolce Mauro, Nicoletti Mario, De Sortis Adriano, Marchesini Sara, Spina Daniele, Talanas Francesco. Osservatorio sismico delle strutture: the Italian structural seismic monitoring network. Bull Earthq Eng 2017;15(2):621–41. https://doi.org/10.1007/s10518-015-9738-x.

[44] Dolce Mauro, Prota Andrea, Borzi Barbara, da Porto Francesca, Lagomarsino Sergio, Magenes Guido, Moroni Claudio, Penna Andrea, Polese Maria, Speranza Elena, Verderame Gerardo Mario, Zuccaro Giulio. Seismic risk assessment of residential buildings in Italy. Bull Earthq Eng 2021;19(8):2999–3032. https://doi.org/10.1007/s10518-020-01009-5.

[45] Elenas Anaxagoras, Meskouris K. Correlation study between seismic acceleration parameters and damage indices of structures. Eng Struct 2001;23:698–704. https://doi.org/10.1016/S0141-0296(00)00074-2.

[46] EN 1998-1:2004. 2004. 'Eurocode 8: Design of Structures for Earthquake Resistance - Part 1: General Rules, Seismic Actions and Rules for Buildings. Brussels, Belgium: European Committee for Standardization'.

[47] Fajfar Peter. Analysis in seismic provisions for buildings: past, present and future. Bull Earthq Eng 2018;16(7):2567–608. https://doi.org/10.1007/s10518-017-0290-8.

[48] FEMA. 2022. 'HAZUS-MH Advanced Engineering Building Module (AEBM) Technical and User's Manual'.

[49] Galvis Francisco, Hulsey Anne, Baker Jack, Deierlein Gregory. Simulation-based methodology to identify damage indicators and safety thresholds for Post-earthquake evaluation of structures. Earthq Eng Struct Dyn 2023;52(11). https://doi.org/10.1002/eqe.3876.

[50] Gattesco N., Franceschinis R., Zorzini F. (2011). 'Metodologia per La Stima Della Resistenza Sismica Degli Edifici Esistenti in Muratura'. in ANIDIS - XIV Convegno Nazionale "L'Ingegneria Sismica in Italia". Bari, Italy.

[51] Gattesco Natalino, Franceschinis Rita, Zorzini Fabio. Numerical procedure for the assessment of seismic vulnerability of masonry buildings. Int J Build Sustain Secur 2014;1(1):35–53. https://doi.org/10.14311/BSS.2014.0005.

[52] Gioiella L, Morici M, Dall'Asta A. Empirical predictive model for seismic damage and economic losses of Italian school building heritage. Int J Disaster Risk Reduct 2023;91:103631. https://doi.org/10.1016/j.ijdrr.2023.103631.

[53] Giusto S, Boem I, Alfano S, et al. Derivation of seismic fragility curves through mechanical-analytical approaches: the case study of the URM school buildings in Friuli-Venezia giulia region (Italy). Bull Earthq Eng 2025;23:2611–46. https://doi.org/10.1007/s10518-025-02137-6.

[54] Giusto S, Cattari S, Lagomarsino S. Investigating the reliability of nonlinear static procedures for the seismic assessment of existing masonry buildings. Appl Sci 2024;14(3):1130. https://doi.org/10.3390/app14031130.

[55] Graziotti F., Magenes G., Penna A. (2012). Experimental Cyclic Behaviour of Stone Masonry Spandrels. in Proceedings of the 15th world conference on earthquake engineering, 15WCEE. Lisbon, Portugal.

[56] Grunthal, G. 1998. 'EMS98 - European Macroseismic Scale 1998, Conseil de l'Europe - Cahiers Du Centre Européen de Géodynamique et de Séismologie, Luxemburg'.

[57] Haddad J, Cattari S, Lagomarsino S. Use of the model parameter sensitivity analysis for the probabilistic-based seismic assessment of existing buildings. Bull Earthq Eng 2019;17:1983–2009. https://doi.org/10.1007/s10518-018-0520-8.

[58] Iervolino I, Galasso C, Cosenza E. REXEL: computer aided record selection for Code-Based seismic structural analysis. Bull Earthq Eng 2009;8(2):339–62. https://doi.org/10.1007/s10518-009-9146-1.
[59] Iervolino I, Galasso C, Paolucci R, Pacor F. Engineering ground motion record selection in the Italian ACcelerometric archive. Bull Earthq Eng 2011;9:1761–78. https://doi.org/10.1007/s10518-011-9300-4.
[60] Iervolino I, Rosti A, Penna A, Giorgio M. Damage-Informed ground motion and Semi-Empirical fragility assessment. Earthq Eng Struct Dyn 2024;53(11): 3514–26. https://doi.org/10.1002/eqe.4184.
[61] Italian Civil Protection Department (2018). 'National Risk Assessment 2018. Overview of the Potential Major Disasters in Italy.'
[62] Jalayer F, Cornell C. Alternative Non-Linear demand estimation methods for Probability-Based seismic assessments. Earthq Eng Struct Dyn 2009;38:951–72. https://doi.org/10.1002/eqe.876.
[63] Jalayer F, Risi R, Manfredi G. Bayesian cloud analysis: efficient structural fragility assessment using linear regression. Bull Earthq Eng 2014;13:1183–203. https://doi.org/10.1007/s10518-014-9692-z.
[64] Karafagka Stella, Fotopoulou Stavroula, Pitilakis Dimitris. Fragility curves of Non-Ductile RC frame buildings on saturated soils including liquefaction effects and Soil–Structure interaction. Bull Earthq Eng 2021;19(12):111629. https://doi.org/10.1007/s10518-021-01081-5.
[65] Katsanos EI, Sextos AG, Manolis GD. Selection of earthquake ground motion records: a state-of-the-art review from a structural engineering perspective. Soil Dynam Earthq Eng 2010;30. https://doi.org/10.1016/j.soildyn.2009.10.005.
[66] Kita Alban, Cavalagli Nicola, Masciotta Maria, Lourenco Paulo, Ubertini Filippo. Rapid Post-Earthquake damage localization and quantification in masonry structures through multidimensional Non-Linear seismic IDA. Eng Struct 2020; 219:110841. https://doi.org/10.1016/j.engstruct.2020.110841.
[67] Kržan Meta, Gostič Samo, Cattari Serena, Bosiljkov Vlatko. Acquiring reference parameters of masonry for the structural performance analysis of historical buildings. Bull Earthq Eng 2015;13(1). https://doi.org/10.1007/s10518-014-9686-x.
[68] Kustu, O., D.D. Miller, and S.T. Brokken. 1982. Development of Damage Functions for High-Rise Building Components. San Francisco, Prepared by URS/John A. Blume & Associates for the U.S. Department of Energy.
[69] Lagomarsino, Sergio. 2022. 'The MARS Vulnerability Model: A New Metrics Based on EMS-98 Vulnerability Classes'. in 3rd EUROPEAN CONFERENCE ON EARTHQUAKE ENGINEERING & SEISMOLOGY. Bucharest, Romania.
[70] Lagomarsino Sergio, Cattari Serena, Ottonelli Daria. The heuristic vulnerability model: fragility curves for masonry buildings. Bull Earthq Eng 2021;19(4): 3129–63. https://doi.org/10.1007/s10518-021-01063-7.
[71] Lagomarsino Sergio, Cattari Serena, Angiolilli Michele, Bracchi Stefano, Rota Maria, Penna Andrea. Modelling and seismic response analysis of existing URM structures. Part 2: archetypes of Italian historical buildings. J Earthq Eng 2022;27(1):1–26. https://doi.org/10.1080/13632469.2022.2087800.
[72] Lagomarsino, Sergio, and Serena Cattari. 2014. 'Fragility Functions of Masonry Buildings'. Pp. 111–56 in SYNER-G: Typology Definition and Fragility Functions for Physical Elements at Seismic Risk, Geotechnical, Geological and Earthquake Engineering. Vol. 27. K. Pitilakis et al. (eds.).
[73] Lagomarsino Sergio, Cattari Serena. PERPETUATE guidelines for seismic Performance-Based assessment of cultural heritage masonry structures. Bull Earthq Eng 2015;13(1):13–47. https://doi.org/10.1007/s10518-014-9674-1.
[74] Lagomarsino Sergio, Cattari Serena. Seismic performance of historical masonry structures through pushover and nonlinear dynamic analyses. Geotech Geol Earthq Eng 2015;39:265–92. https://doi.org/10.1007/978-3-319-16964-4_11.
[75] Lagomarsino S, Giovinazzi S. Macroseismic and mechanical models for the vulnerability and damage assessment of current buildings. Bull Earthq Eng 2006; 4:415–43. https://doi.org/10.1007/s10518-006-9024-z.
[76] Lagomarsino Sergio, Penna Andrea, Galasco Alessandro, Cattari Serena. TREMURI program: an equivalent frame model for the nonlinear seismic analysis of masonry buildings. Eng Struct 2013;56:1787–99. https://doi.org/10.1016/j.engstruct.2013.08.002.
[77] Luco Nicolas, Cornell CAllin. Structure-Specific scalar intensity measures for near-source and ordinary earthquake ground motions. Earthq Spectra 2007;23 (2):357–92. https://doi.org/10.1193/1.2723158.
[78] Manfredi Vincenzo, Masi Angelo, Özcebe Ali Güney, Paolucci Roberto, Smerzini Chiara. Selection and spectral matching of recorded ground motions for seismic fragility analyses. Bull Earthq Eng 2022;20(10):4961–87. https://doi.org/10.1007/s10518-022-01393-0.
[79] Marino Salvatore, Cattari Serena, Lagomarsino Sergio. Are the nonlinear static procedures feasible for the seismic assessment of irregular existing masonry buildings? Eng Struct 2019;200:109700. https://doi.org/10.1016/j.engstruct.2019.109700.
[80] Martineau Gordon Martin, Lopez Alvaro, Vielma Juan. Effect of earthquake ground motion duration on the seismic response of a Low-Rise RC building. Adv Civ Eng 2020;2020(5):1–12. https://doi.org/10.1155/2020/8891282.
[81] Martins Luis, Silva Vitor, Marques Mário, Crowley Helen, Delgado Raimundo. Development and assessment of Damage-to-Loss models for Moment-Frame reinforced concrete buildings. Earthq Eng Struct Dyn 2015;45(5):797–817. https://doi.org/10.1002/eqe.2687.
[82] Masi Angelo, Lagomarsino Sergio, Dolce Mauro, Manfredi Vincenzo, Ottonelli Daria. Towards the updated Italian seismic risk assessment: exposure and vulnerability modelling. Bull Earthq Eng 2021;19(8):3253–86. https://doi.org/10.1007/s10518-021-01065-5.
[83] Masi, Angelo, Sergio Lagomarsino, Vincenzo Manfredi, and Giuseppe Nicodemo. 2022. 'The Italian Seismic Risk Maps: An Overview of the Methodology and Results of MARS Project'. in 3rd EUROPEAN CONFERENCE ON EARTHQUAKE ENGINEERING & SEISMOLOGY. Bucharest, Romania.
[84] Minas Stylianos, Galasso Carmine. Accounting for spectral shape in simplified fragility analysis of case-study reinforced concrete frames. Soil Dyn Earthq Eng 2019;119:91–103. https://doi.org/10.1016/j.soildyn.2018.12.025.
[85] Mollaioli F, Lucchini A, Cheng Y, Monti G. Intensity measures for the seismic response prediction of Base-Isolated buildings. Bull Earthq Eng 2013;11(5): 1841–66. https://doi.org/10.1007/s10518-013-9431-x.
[86] Monteferrante Chiara, Cattari Serena, D'Altri Antonio, Castellazzi Giovanni, Lagormarsino S, Miranda Stefano. 'An energy-based methodology to estimate the ultimate condition of complex continuous masonry structures'. Eng Fail Anal 2023;151:107370. https://doi.org/10.1016/j.engfailanal.2023.107370.
[87] Morandi Paolo, Albanesi Luca, Graziotti Francesco, Li Piani Tiziano, Penna Andrea, Magenes Guido. Development of a dataset on the In-Plane experimental response of URM piers with bricks and blocks. Constr Build Mater 2018;190:593–611. https://doi.org/10.1016/j.conbuildmat.2018.09.070.
[88] Mori Federico, Spina Daniele, Bocchi Flavio, Mendicelli Amerigo, Naso Giuseppe, Moscatelli Massimiliano. Machine learning model for building seismic peak roof drift ratio assessment. Geomat Nat Hazards Risk 2023;14(1):2182658. https://doi.org/10.1080/19475705.2023.2182658.
[89] Mouyiannou Amaryllis, Rota Maria, Penna Andrea, Magenes Guido. Identification of suitable limit states from nonlinear dynamic analyses of masonry structures. J Earthq Eng 2014;18(2):231–63. https://doi.org/10.1080/13632469.2013.842190.
[90] Nakamura Yasuto, Derakhshan Hossein, Griffith M, Magenes Guido. Influence of diaphragm flexibility on seismic response of unreinforced masonry buildings. J Earthq Eng 2016;21(6):935–60. https://doi.org/10.1080/13632469.2016.1190799.
[91] Nettis A, Gentile R, Raffaele D, et al. Cloud capacity spectrum method: accounting for Record-to-Record variability in fragility analysis using nonlinear static procedures. Soil Dyn Earthq Eng 2021;150:106829. https://doi.org/10.1016/j.soildyn.2021.106829.
[92] NTC. 2018. 'Decreto Ministeriale 17/1/2018. Norme Tecniche per Le Costruzioni. Rome, Italy: Ministry of Infrastructures and Transportations'.
[93] OAK. 1994. Development of Damage Functions for Buildings, OAK Engineering Inc.
[94] Ottonelli, Daria, Sara Alfano, Serena Cattari, Marco Di Ludovico, and Andrea Prota. 2019. 'Analisi Statistiche Dei Dati Tipologici e Di Danno Delle Scuole in Muratura Danneggiate Dal Terremoto Del Centro Italia 2016/2017'. in XVIII Convegno ANIDIS, L'ingegneria Sismica in Italia. Ascoli Piceno, Italia.
[95] Palanci Mehmet, Demir Ahmet, Kayhan Ali Haydar. Quantifying the effect of amplitude scaling of real ground motions based on structural responses of vertically irregular and regular RC frames. Structures 2023;51:105–23. https://doi.org/10.1016/j.istruc.2023.03.040.
[96] Penna Andrea, Rota Maria, Bracchi Stefano, Angiolilli Michele, Cattari Serena, Lagomarsino Sergio. Modelling and seismic response analysis of existing URM structures. Part 1: archetypes of Italian modern buildings. J Earthq Eng 127 2022. https://doi.org/10.1080/13632469.2022.2095060.
[97] Penna Andrea, Senaldi Ilaria, Galasco Alessandro, Magenes Guido. Numerical simulation of shaking table tests on Full-Scale stone masonry buildings. Int J Archit Herit 2016;10(2–3):146–63. https://doi.org/10.1080/15583058.2015.1113338.
[98] Petracca M, Camata G, Spacone E, Pelà L. Efficient constitutive model for continuous Micro-Modeling of masonry structures. Int J Archit Herit 2022;17(1): 134–46. https://doi.org/10.1080/15583058.2022.2124133.
[99] Petry Sarah, Beyer Katrin. Influence of boundary conditions and size effect on the drift capacity of URM walls. Eng Struct 2014;65:76–88. https://doi.org/10.1016/j.engstruct.2014.01.048.
[100] Phadnis P, Desai R, Tande S, Dhumal P. Fragility analysis of masonry infill R.C. Frame using incremental dynamic approach. Asian J Civ Eng 2023;24. https://doi.org/10.1007/s42107-023-00719-w.
[101] Pinasco, Silvia, M. Demšić, A. Pilipović, M.Šavor Novak, M. Uroš, Sergio Lagomarsino, and Serena Cattari. 2024. 'Seismic Fragility Assessment of Existing Masonry Buildings in Aggregate Located in Zagreb'. Bulletin of Earthquake Engineering.
[102] Polese M, Tocchi G, Babič A, et al. Multi-Risk assessment in transboundary areas: a framework for harmonized evaluation considering seismic and flood risks. Int J Disaster Risk Reduct 2024;101:104275. https://doi.org/10.1016/j.ijdrr.2024.104275.
[103] Rezaie Amir, Godio Michele, Beyer Katrin. Experimental investigation of strength, stiffness and drift capacity of rubble stone masonry walls. Constr Build Mater 2020;251:118972. https://doi.org/10.1016/j.conbuildmat.2020.118972.
[104] Rossetto Tiziana, D'Ayala Dina, Ioannou Ioanna, Meslem Abdelghani. 'Evaluation of existing fragility Curves'. pp. 47–93 In SYNER-G: typology definition and fragility functions for physical elements at seismic risk. Geotechnical. Geological and Earthquake Engineering, 27. Netherlands: Springer; 2014.
[105] Rossetto, Tiziana, Ioanna Ioannou, and Damian Grant. 2015. Existing Empirical Fragility and Vulnerability Functions: Compendium and Guide for Selection. 2015–1. GEM Technical Report. doi: 10.13117/GEM.VULNSMOD.TR2015.01.
[106] Rosti A, Rota M, Penna A. Empirical fragility curves for Italian URM buildings. Bull Earthq Eng 2021;19:3057–76. https://doi.org/10.1007/s10518-020-00845-9.
[107] Ruggieri S, Liguori SF, Leggieri V, et al. An Archetype-Based automated procedure to derive Global-Local seismic fragility of masonry building aggregates: META-FORMA-XL. Int J Disaster Risk Reduct 2023;95:103903. https://doi.org/10.1016/j.ijdrr.2023.103903.

[108] Ruggieri Sergio, Uva Giuseppina. Accounting for the spatial variability of seismic motion in the pushover analysis of regular and irregular RC buildings in the new Italian building code. Buildings 2020;10(10):177. https://doi.org/10.3390/buildings10100177.
[109] Saler E., Follador V., Carpanese P., da Porto F. (2021). Fragility Assessment of the Italian Masonry School Building Asset for Risk Evaluation at National Scale. Pp. 3113–26 in COMPDYN - 8th ECCOMAS Thematic Conference on Computational Methods in Structural Dynamics and Earthquake Engineering Methods in Structural Dynamics and Earthquake Engineering. Athens, Greece.
[110] Sandoli A, Brandonisio G, Lignola GP, Prota A, Fabbrocino G. Seismic fragility matrices for large scale probabilistic structural safety assessment. Soil Dyn Earthq Eng 2023;171:107963. https://doi.org/10.1016/j.soildyn.2023.107963.
[111] Sandoli A, Lignola GP, Calderoni B, Prota A. Fragility curves for Italian URM buildings based on a hybrid method. Bull Earthq Eng 2021;19(12):4979–5013. https://doi.org/10.1007/s10518-021-01155-4.
[112] Sgobba S., Puglia R., Pacor F., et al. (2019). REXELweb: A Tool for Selection of Ground-Motion Records from the Engineering Strong Motion Database (ESM). in 7th International Conference on Earthquake Geotechnical Engineering. Rome, Italy.
[113] Shome N. (1999). Probabilistic Seismic Demand Analysis of Nonlinear Structures. PhD Thesis, Stanford University, California.
[114] Silva V, Amo-Oduro D, Calderon A, Costa C, et al. Development of a global seismic risk model. Earthq Spectra 2020;36(1_):372–94. https://doi.org/10.1177/8755293019899953.
[115] Silva V, Crowley H, Pinho R, Varum H. Extending Displacement-Based earthquake loss assessment (DBELA) for the computation of fragility curves. Eng Struct 2013;56:343–56. https://doi.org/10.1016/j.engstruct.2013.04.023.
[116] Simões Ana, Bento Rita, Lagomarsino Sergio, Cattari Serena, Lourenço Paulo B. Fragility functions for tall URM buildings around early 20th century in Lisbon. Part 1: methodology and application at building level. Int J Archit Herit 2019;15(3):349–72. https://doi.org/10.1080/15583058.2019.1618974.
[117] Sivori Daniele, Cattari Serena, Lepidi Marco. A methodological framework to relate the Earthquake-Induced frequency reduction to structural damage in masonry buildings. Bull Earthq Eng 2022;20(8):4603–38. https://doi.org/10.1007/s10518-022-01345-8.
[118] Sivori D, Lepidi M, Cattari S. Structural identification of the dynamic behavior of floor diaphragms in existing buildings. Smart Struct Syst 2021;27(2):173–91. https://doi.org/10.12989/sss.2021.27.2.173.
[119] Smerzini C, Amendola C, Paolucci R, Bazrafshan A. Engineering validation of BB-SPEEDset, a data set of near-Source Physics-Based simulated accelerograms. Earthq Spectra 0 2023. https://doi.org/10.1177/87552930231206766.
[120] Smerzini C, Galasso C, Iervolino I, Paolucci R. Ground motion record selection based on broadband spectral compatibility. Earthq Spectra 2014;30(4):1427–48. https://doi.org/10.1193/052312EQS197M.
[121] Smerzini, Chiara, and Roberto Paolucci. 2013. 'SIMBAD: A Database with Selected Input Motions for Displacement Based Assessment and Design – 3rd Release by Department of Structural Engineering'.
[122] Sucuoğlu Halûk, Eren Numan, Pinho Rui. Interstory drift based scaling of Bi-Directional ground motions. Earthq Eng Struct Dyn 2022;51(15):3620–38. https://doi.org/10.1002/eqe.3739.
[123] Ulrich Thomas, Negulescu Caterina, Douglas John. Fragility curves for Risk-Targeted seismic design maps. Bull Earthq Eng 2013;12(4):1479–91. https://doi.org/10.1007/s10518-013-9572-y.
[124] Vamvatsikos D, Cornell C. Incremental dynamic analysis. Earthq Earthq Eng Struct Dyn 2002;31:491–514. https://doi.org/10.1002/eqe.141.
[125] Vamvatsikos D, Cornell C. Direct estimation of the seismic demand and capacity of oscillators with Multi-Linear static pushovers through IDA. Earthq Eng Struct Dyn 2006;35(9):1097–117. https://doi.org/10.1002/eqe.573.
[126] Vanin F, Penna A, Beyer K. A Three-Dimensional macroelement for modelling the in-Plane and out-of-Plane response of masonry walls. Earthq Eng Struct Dyn 2020;49(14):1365–87. https://doi.org/10.1002/eqe.3277.
[127] Vanin F, Zaganelli D, Penna A, Beyer K. Estimates for the stiffness, strength and drift capacity of stone masonry walls based on 123 Quasi-Static cyclic tests reported in the literature. Bull Earthq Eng 2017;15:5435–79. https://doi.org/10.1007/s10518-017-0188-5.
[128] Vicente R, Parodi S, Lagomarsino S, Varum H, Silva RM. Seismic vulnerability and risk assessment: case study of the historic city centre of coimbra, Portugal. Bull Earthq Eng 2011;9(4):1067–96. https://doi.org/10.1007/s10518-010-9233-3.
[129] Zuccaro G, Perelli F, De Gregorio D, Cacace F. Empirical vulnerability curves for Italian mansory buildings: evolution of vulnerability model from the DPM to curves as a function of accelertion. Bull Earthq Eng 2021;19(3):1–21. https://doi.org/10.1007/s10518-020-00954-5.
[130] Zucconi Maria, Bovo Marco, Ferracuti Barbara. Fragility curves of existing RC buildings accounting for bidirectional ground Motion'. Buildings 2022;12(7). https://doi.org/10.3390/buildings12070872.3.